New acetylene line list near 3.8-μm – Part II

David Jacquemart, O.M. Lyulin, A.M. Solodov, T.M. Petrova, A.A. Solodov

New acetylene line list near 3.8-μm - Part II

D. Jacquemart [a,*], O.M. Lyulin[b], A.M. Solodov[b], T.M. Petrova[b] and A.A. Solodov[b]

[a] Sorbonne Université, CNRS, MONARIS, UMR 8233, 4 place Jussieu, 75005 Paris, France

[b] V.E. Zuev Institute of Atmospheric Optics, Siberian Branch, Russian Academy of Sciences,1, Academician Zuev Square, 634055 Tomsk, Russia

Number of Figures: 12
Number of Tables: 4
Supplementary materials (electronic files): 2

Please send proofs to: David Jacquemart
Email: david.jacquemart@upmc.fr

Keywords : Acetylene; Measured line positions and intensities; Spectroscopic constants; Global modelling; Line list; Spectroscopic databases.

Abstract

The investigation of the 3.8 μm spectral region of acetylene $^{12}C_2H_2$ main isotopologue has been completed from spectra recorded with Fourier Transform Spectrometer (FTS) using high optical path length. This work is the second of a series dedicated to the $\Delta P = 4$ spectral region. In the first paper of the series (JQSRT 2023;295:108413) 14 bands of $^{12}C_2H_2$ were studied in the beginning of the region. In the present work the whole $\Delta P = 4$ spectral region was investigated. 52 newly observed vibrational bands have been studied as well as the 5 intense bands present in the HITRAN and GEISA databases. The band centers and the upper level spectroscopic constants were retrieved for all bands. The comparison with the data from HITRAN and GEISA databases revealed important deviations from the measurements due to wrong extrapolations (especially line positions). The effective dipole moment operator parameters describing intensities of all transitions observed in the $\Delta P = 4$ spectra region were refined. A complete list of calculated line parameters for 7515 transitions has been generated for 71 bands between 2389 cm^{-1} and 2890 cm^{-1}.

1. Introduction

This paper is the second of the series dedicated to the investigation of the spectral region near 3.8-μm under large experimental absorption paths conditions. In the first work [1] of the series 14 bands of $^{12}C_2H_2$ were studied in the beginning of the $\Delta P = 4$ spectral region whereas the whole region could not be analyzed due to the edge of the optical filter used in Ref. [1]. P is the polyad number defined as $P = 5V_1 + 3V_2 + 5V_3 + V_4 + V_5$, where V_i are the vibrational normal mode principal quantum numbers, with $i = 1-5$. In the present work no optical filter was used allowing to investigate 57 other bands including the 5 intense bands present in databases.

The $\Delta P = 4$ spectral region was previously studied in Ref. [2]. In result of that investigation 421 lines of the 5 bands were posted in spectroscopic databases. In Ref. [3] the set of 8 effective dipole moment parameters for this region was reported. In our previous work [1] the ASD-1000 database [4] based on the effective operators proposed in Ref. [5] has been used to assign 824 transitions of 14 bands never measured before in the low part of the region. Note that for some of the newly observed bands predicted line positions issued from Ref. [4] appeared shifted from the observations with deviations up to 0.1 cm^{-1}. The new observations [1] allowed retrieving the set of the spectroscopic constants describing upper levels of the corresponding bands. For several bands the comparisons between measured and calculated line positions showed deviations for high rotational quantum number J appearing due to resonance interactions between levels. The line positions in the final line list were calculated using spectroscopic constants. For the line intensities no attempt has been done to use Herman-Wallis factors to reproduce the rotational dependences of the observed transition dipole moments squared since such procedure fails in many cases (see Ref. [1]). On the contrary the predicted using effective dipole moment (EDM) parameters line intensities, where mixing of the states is taken into account, reproduced very well the rotational dependence of the observed transition dipole moments squared. As a consequence only the calculations with refined EDM parameters were used to generate line intensities in the generated line list of Ref. [1].

The present paper is devoted to the analysis of spectra recorded without optical filter in order to compile a full $^{12}C_2H_2$ line list giving the best agreement between the simulating spectra and the observations in the whole ΔP=4 spectral region. The experimental setup and conditions are presented in Section 2. A brief description of the measurements is given in Section 3. The band-by-band rotational analysis leading to spectroscopic parameters is presented in Section 4. The measurements are compared to the predictions of the EH and calculations using spectroscopic parameters in the same section. The new set of the EDM parameters is presented

in the Section 5. The details of the final line list construction for $^{12}C_2H_2$ in the $\Delta P = 4$ spectral region are given in Section 6.

2. Experimental procedure

Three Fourier transform spectra were recorded using Bruker IFS-125HR spectrometer connected to the White type cell with the base length of 27.795 m built in the V.E. Zuev Institute of Atmospheric Optics SB RAS. The spectra were recorded with a pressure of pure acetylene equal to 0.997 matm and absorption path lengths of 168.51, 613.23 and 1057.95 m. The temperature of the gas in the cell measured by platinum probe was equal to 301.4-301.6 K depending on spectrum. The spectral resolution was equal to 0.005 cm^{-1}, corresponding to a maximum optical path difference of 180 cm. The instrument was fitted with a tungsten source, a 1.15 mm entrance aperture (diameter) together with a collimator focal length of 418 mm, a KBr beam splitter and an MCT detector (no non-linear correction from MCT detector was performed). The acetylene commercial sample was used without purification (95% of C_2H_2 with traces of CH_4 (~ 0.1 %) and PH_3 (~ 0.1%), CO_2 (~ 0.04%) and acetone as impurities) and is different to the one used in Ref. [1]. No artificial optical weighting has been performed (boxcar function was selected). A Mertz procedure was used to correct phase of average interferogram. The *R*(64) to *R*(78) transitions of the ν_3 band of carbon dioxide (presents in the cell as impurity) have been used for the wavenumber calibration (via HITRAN wavenumbers as etalons). The RMS deviation of the wavenumber calibration is equal to 0.1×10^{-3} cm^{-1}. Note that an error in the calibration of spectra from Ref. [1] led to systematic deviation of 0.8×10^{-3} cm^{-1} in the positions retrieved in Ref. [1]. This mistake has been fixed in the present work so that line positions measured in the whole $\Delta P = 4$ spectral regions are consistent with accuracy better than 10^{-3} cm^{-1}.

3. Line parameters measurements

As in our previous work the ASD-1000 line list [4] allowed assigning the majority of the transitions observed in our spectra. However, systematical deviations were observed so the predictions were rescaled in order to be used as initial guess. The multispectrum fitting procedure [6] has then been applied to the three experimental spectra recorded in the present work in order to retrieve line positions and intensities fixing the self-widths to the values of the HITRAN database [7]. The Voigt profile has been used together with the calculated instrument line shape (ILS) describing the effects of the limited optical path difference and of the size of the beam inside the interferometer (see Ref. [8]). The assignment allowed performing the

conversion of the intensities to the standard temperature 296K using lower state energies from ASD-1000 line list [4] and partition function from Ref. [9]. An example of the multispectrum fitting performed in the present work is given in Fig. 1 between 2688.446 and 2688.632 cm^{-1}.

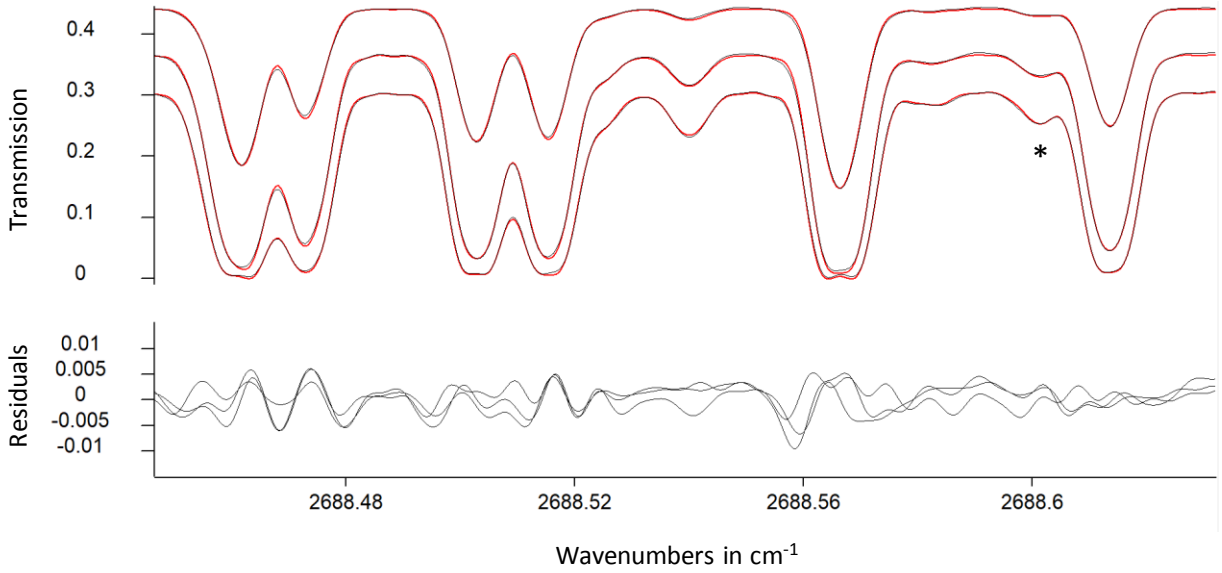

Fig. 1. Observed (black) and calculated (red) spectra (together with residuals obs-calc) between 2688.446 and 2688.632 cm^{-1}. The fitted line noted with a star is a $^{12}C^{13}H_2$ transition, all others transitions are from $^{12}C_2H_2$ and are studied for the first time.

The present work includes measurements for 71 bands, 52 among them were studied for the first time. For the 5 bands studied in Ref. [2] and present in HITRAN [7] or GEISA [10] databases the new measurements allowed to reach higher *J* values. Note that in Ref. [2] and in HITRAN and GEISA databases, the upper state of the $(\nu_2+(\nu_4+\nu_5)^0 - \nu_4^1)$ band is wrongly written with $\ell_4 = \ell_5 = 0$ instead of $\ell_4 = -\ell_5 = 1$ (namely 010 1 1 0 0_000 1 0 1 0 instead of 010 1 1 1-1_000 1 0 1 0). Moreover, the upper states of the $(\nu_3 - \nu_4^1)$ and $(\nu_2+(\nu_4+\nu_5)^0 - \nu_4^1)$ bands have similar contributions of the base functions making thus the vibrational assignment ambiguous. In the present work, we used the vibrational notation adopted in ASD-1000 [4] where the notation for these two bands is reversed comparing to the notation given in the HITRAN and GEISA databases and in Ref. [2]. The 14 bands observed in Ref. [1] have been reinvestigated only in term of line positions in order to improve the rotational analysis of the energy levels. The accuracy of measurements is estimated to be better than 0.001 cm^{-1} for line positions and between 5 and 10 % for most of the line intensities. As explained in Ref. [1], for some bands the largest contributions of the harmonic oscillators basis states to the predicted upper or lower states, considering as function of *J*, intersect, making ambiguous the vibrational assignment after crossings. In such cases we use the same vibrational labeling for a series of transitions, keeping the regularity of the rotational transitions inside the bands (see section 5 of

Ref. [11] for the details). The whole set of measurements performed in this work is given as Supplementary Material I, containing 5092 line positions and 2674 line intensities (note that for the 14 bands studied in Ref. [1] only line positions have been reinvestigated in the present work). For blended, saturated or very weak transitions the line intensity measurements are not accurate and have been ignored whereas the line positions have been conserved. Note that the accuracy of line positions for the saturated or non saturated transitions is similar since a profile is fitted.

4. Line positions: band-by-band rotational analysis

In order to accurately reproduce and interpolate measurements the measured line positions were fitted using the following equation for the energies of the levels written up to eighth order of perturbation theory:

$$T(v, J, e/f) = G_{e/f} + B_{e/f}J(J+1) - D_{e/f}[J(J+1)]^2 + H_{e/f}[J(J+1)]^3 + L_{e/f}[J(J+1)]^4 + M_{e/f}[J(J+1)]^5. \quad (1)$$

Although the energy of an unperturbed state is usually described with a fewer amount of spectroscopic parameters, in order to reach satisfactory residuals for the perturbed state it is required more parameters. The spectroscopic constants of the lower vibrational levels have been fixed to the values given in Refs. [12,13] (except for the $V_2 = 1$ level fitted from Ref. [14], see Table 1). The different sets of the spectroscopic constants were fitted for *e* and *f* sublevels assuming different perturbing mechanism for them. The defined spectroscopic constants allowed reproduce the most of the observed line positions with RMS within 0.001-0.002 cm^{-1} depending on the band. For some bands the oscillations in obs-calc residuals are observed. The description of such perturbed bands by spectroscopic constants is then valid only up to a certain *J* value starting from which the deviations dramatically increase. Therefore some line positions measured for high *J* values were excluded from the fit. The spectroscopic constants retrieved in this work are given in the Table 1.

Table 1. Spectroscopic parameters (in cm^{-1}) of the rovibrational bands of acetylene assigned in the FTS spectra in the *ΔP=4* region. The bands are listed according to the increasing values of the upper state energy.

$V_1V_2V_3V_4V_5\ \ell_4\ \ell_5\varepsilon$ [a]	$G_{e/f}$	$B_{e/f}$	$D_{e/f}\times10^6$	$H_{e/f}\times10^9$	$L_{e/f}\times10^{11}$	$M_{e/f}\times10^{14}$	n_{fit}/N_{tot} [b]	ΔG [c]	Bands [d]	*Rms* [e]
Lower vibrational levels **[12,13]**										
00000 0 0e	0.0	1.1766462	1.6270	0.0016						
00010 1 0f	611.693755	1.18055377	1.67973	0.00187						
00010 1 0e	611.693759	1.17532307	1.6405	0.00177						
00001 0 1e	729.15410	1.1764413	1.6326	0.0017						
00001 0 1f	729.15410	1.1811398	1.6714	0.0018						
00011 1-1e	1328.0722	1.180508	3.595	0.276						
00020 2 0f	1228.7997	1.179109	1.692							
00020 2 0e	1228.8011	1.17908	19.0	2.45						
00020 0 0e	1230.3894	1.17937	-15.8	-2.46						
00011 1-1f	1340.5507	1.1800836	1.715							
00011 1 1f	1342.8023	1.179838	1.647							
00011 1 1e	1342.8034	1.179804	-0.226	-0.278						
00002 0 0e	1449.1107	1.181234	4.415	0.652						
00002 0 2f	1458.2936	1.180757	1.669							
00002 0 2e	1458.2944	1.180714	-1.052	-0.643						
00030 3 0e	1851.3699	1.180358	10.15							
00030 3 0f	1851.3749	1.18006	6.33	3.9						
00030 1 0f	1854.5970	1.18583	-3.8	-6.1						
00030 1 0e	1854.5978	1.17533	-6.2							
00021 2-1f	1939.9987	1.185710	3.065							
00021 2-1e	1939.9999	1.177984	2.867	0.165						
00021 0 1e	1959.6916	1.182691	3.22							
00021 0 1f	1959.6921	1.179939	3.23	0.6						
00021 2 1f	1961.9321	1.180731	-1.03	-0.515						
00021 2 1e	1961.9332	1.18069	-1.31	-1						
01000 0 0e [f]	1974.31610(2)	1.1704678(2)	1.6321(6)	0.0033(4)						
00012 1 2e	2074.1790	1.181561	1.056							
00012 1 2f	2074.1807	1.181533	0.95	0.17						
00012 1 0f	2047.8761	1.187537	2.592	-0.148						
00012 1 0e	2047.8766	1.177928	2.457	0.113						
00012-1 2f	2065.7923	1.184239	1.672							
00012-1 2e	2065.7929	1.180042	1.618							
00003 0 1f	2169.1559	1.188211	2.782	-0.189						
00003 0 1e	2169.1575	1.178631	2.550	0.165						
00003 0 3e	2187.4505	1.182540	0.86							
00003 0 3f	2187.4521	1.182494	0.56							

Upper vibrational levels (this work)

	***P*=4**											
	00031 3-1e	2556.7939(7)	1.18318(1)	18.34(8)	20.1(2)	-1.32(2)	0.347(7)	46/49	2556.7939(7)	$(3\nu_4+\nu_5)^2$II	1.0	
	00031 1-1e	2560.5946(4)	1.183264(9)	-12.66(5)	-19.1(1)	1.20(1)	-0.304(4)	61/61	2560.5946(4)	$(3\nu_4+\nu_5)^0$	1.7	
	00031 1 1e	2585.046(4)	1.18166(3)	5.16(7)	2.16(5)			8/8	2585.046(4)	$(3\nu_4+\nu_5)^2$I	0.7	
	01001 0 1e	2701.9098(2)	1.1702027(7)	1.6306(4)				77/77	2701.9098(2)	$\nu_2 + \nu_5^1$	0.3	
	01001 0 1f	2701.9109(9)	1.174895(2)	1.667(1)				27/27	2701.9109(9)	$\nu_2 + \nu_5^1$	0.2	
	00013 1-1e	2757.7974(6)	1.18532(1)	9.06(8)	2.3(1)			26/26	2757.7974(6)	$(\nu_4+3\nu_5)^0$	0.3	
	***P*=5**											
	01020 2 0f	3178.7269(5)	1.172773(5)	1.67(1)				24/24	2449.5929(5)	$\nu_2 + 2\nu_4^2 - \nu_5^1$	0.4	
	01020 2 0e	3178.746(2)	1.17241(3)	14.8(2)	19.7(4)	-1.47(4)	0.42(1)	44/52	2449.592(2)	$\nu_2 + 2\nu_4^2 - \nu_5^1$	2.0	
N	00041 4-1e	3178.795(3)	1.18550(2)	13.34(5)	4.17(3)			24/25	2567.101(3)	$(4\nu_4+\nu_5)^3$II - ν_4^1	1.2	
N	00041 4-1f	3178.947(3)	1.18348(2)	4.42(3)				10/10	2567.253(3)	$(4\nu_4+\nu_5)^3$II - ν_4^1	1.8	
	01020 0 0e	3180.6544(4)	1.17298(1)	-14.4(1)	-28.5(4)	2.58(5)	-0.93(3)	59/59	2451.5003(4)	$\nu_2 + 2\nu_4^0 - \nu_5^1$	0.9	
	00041 2-1f	3185.4289(4)	1.191690(7)	-1.57(3)	-3.34(4)	0.100(2)		46/46	2573.7351(4)	$(4\nu_4+\nu_5)^1$II - ν_4^1	1.2	
	00041 2-1e	3185.4314(4)	1.17778(1)	-2.12(9)	9.1(3)	-1.30(3)	0.48(1)	45/50	2573.7377(4)	$(4\nu_4+\nu_5)^1$II - ν_4^1	1.9	
	00032 3-2f	3260.6155(3)	1.190996(3)	5.358(5)				44/44	2531.4622(3)	$(3\nu_4+2\nu_5)^1$III - ν_5^1	0.9	
	00032 3-2e	3260.6163(3)	1.180822(4)	4.93(1)	0.647(9)			41/41	2531.4630(3)	$(3\nu_4+2\nu_5)^1$III - ν_5^1	0.8	
	00032 3 0f	3280.608(2)	1.18413(3)	10.1(2)	16.4(7)	-1.68(8)	0.65(4)	32/34	2551.454(2)	$(3\nu_4+2\nu_5)^3$II - ν_5^1	1.7	
	00032 3 0e	3280.612(1)	1.18393(3)	2.7(2)	4.5(5)	-0.32(4)		27/28	2551.458(1)	$(3\nu_4+2\nu_5)^3$II - ν_5^1	1.7	
	00032-1 2e	3280.9573(4)	1.18648(2)	-5.1(2)	-20.2(7)	2.5(1)	-1.18(6)	42/45	2551.8032(4)	$(3\nu_4+2\nu_5)^1$II - ν_5^1	1.8	
	00032-1 2f	3280.9609(5)	1.18432(3)	-16.3(4)	-51(2)	8.1(5)	-5.0(4)	40/47	2551.8068(5)	$(3\nu_4+2\nu_5)^1$II - ν_5^1	1.1	
	00100 0 0e	3281.9004(2)	1.172531(2)	2.416(3)	0.124(1)			110/110	2670.2066(2)	$\nu_3 - \nu_4^1$	1.1	
	01011 1-1e	3294.8385(3)	1.172426(3)	3.235(9)	0.403(9)	-0.0027(3)		109/109	2683.1447(3)	$\nu_2+(\nu_4+\nu_5)^0 - \nu_4^1$	0.9	
	01011 1-1f	3300.6352(2)	1.173779(1)	1.717(1)				73/73	2688.9414(2)	$\nu_2+(\nu_4+\nu_5)^0 - \nu_4^1$	0.2	
	01011 1 1e	3303.0182(3)	1.173510(2)	-0.615(5)	-0.456(2)			60/60	2691.3244(3)	$\nu_2+(\nu_4+\nu_5)^2 - \nu_4^1$	0.7	
	01011 1 1f	3303.0184(2)	1.173524(1)	1.645(1)				77/77	2691.3246(2)	$\nu_2+(\nu_4+\nu_5)^2 - \nu_4^1$	0.5	
	10000 0 0e	3372.8477(2)	1.1698001(7)	1.6123(4)				113/113	2643.6936(2)	$\nu_1 - \nu_5^1$	0.3	
N	01002 0 0e	3420.3850(3)	1.174936(4)	4.56(1)	0.85(1)	-0.0088(4)		79/79	2691.2308(3)	$\nu_2 + 2\nu_5^0 - \nu_5^1$	1.0	
N	01002 0 2f	3429.4133(2)	1.174452(1)	1.6692(9)				86/86	2700.2592(2)	$\nu_2 + 2\nu_5^2 - \nu_5^1$	0.3	
N	01002 0 2e	3429.4141(3)	1.174413(3)	-1.064(6)	-0.648(3)			74/74	2700.2600(3)	$\nu_2 + 2\nu_5^2 - \nu_5^1$	0.8	
	***P*=6**											
N	00051 3-1f	3814.9681(4)	1.185842(7)	-2.49(3)	-1.92(3)			36/36	2586.1670(4)	$(5\nu_4+\nu_5)^2$II - $2\nu_4^2$	0.7	
N	00051 3-1e	3814.9694(7)	1.18586(3)	41.4(3)	66.3(8)			23/35	2586.1683(7)	$(5\nu_4+\nu_5)^2$II - $2\nu_4^2$	0.9	**P**
N	00051 1-1e	3818.0594(6)	1.18625(3)	-41.1(3)	-66(1)			22/30	2587.670(6)	$(5\nu_4+\nu_5)^0 - 2\nu_4^0$	0.7	**P**
	01021 2-1f	3881.2336(3)	1.177463(3)	2.532(7)	0.110(5)			12/26	2650.8442(3)	$\nu_2+(2\nu_4+\nu_5)^1$II - $2\nu_4^0$	0.7	**P**
								57/62	2652.4325(2)	$\nu_2+(2\nu_4+\nu_5)^1$II - $2\nu_4^2$	0.5	**P**
	01021 2-1e	3881.2337(2)	1.170664(3)	2.189(7)	0.076(4)			24/31	2650.8443(2)	$\nu_2+(2\nu_4+\nu_5)^1$II - $2\nu_4^0$	0.6	**P**
								49/80	2652.4326(2)	$\nu_2+(2\nu_4+\nu_5)^1$II - $2\nu_4^2$	0.7	**P**

	00042 2-2e	3883.0585(6)	1.18754(1)	-10.44(9)	-10.9(1)
	00110 1 0f	3897.1612(2)	1.176382(1)	2.505(1)	
	00110 1 0e	3897.1632(2)	1.170674(2)	2.466(4)	
	00042 2-2f	3906.2098(9)	1.18477(3)	5.3(1)	
N	01021 0 1f	3908.1358(8)	1.17381(2)	3.41(6)	
N	01021 0 1e	3908.1363(5)	1.17602(1)	3.25(4)	
N	01021 2 1f	3910.1846(8)	1.17435(2)	-1.43(6)	
N	01021 2 1e	3910.1861(8)	1.17430(2)	-1.92(7)	-1.7(1)
	10010 1 0e	3968.8832(2)	1.1686998(8)	1.6387(8)	
	10010 1 0f	3968.8836(2)	1.1740327(8)	1.6891(8)	
	01012 1 0f	4001.2594(2)	1.178727(3)	2.741(7)	0.125(5)
	01012 1 0e	4001.2600(3)	1.171278(3)	2.096(8)	0.067(5)
	00101 0 1e	4015.5364(2)	1.170794(3)	2.066(7)	0.089(5)
	00101 0 1f	4015.5365(2)	1.177594(2)	1.493(6)	-0.326(4)
N	01012-1 2e	4024.3843(3)	1.177802(3)	1.649(4)	
N	01012-1 2f	4024.3848(3)	1.173597(2)	1.639(3)	
N	01012 1 2f	4032.7087(6)	1.175152(8)	0.87(3)	0.17(3)
N	01012 1 2e	4032.7089(6)	1.175152(8)	0.88(2)	-0.17(2)
	10001 0 1e	4091.1720(2)	1.169604(1)	1.621(1)	
	10001 0 1f	4091.1722(2)	1.174396(1)	1.669(1)	
	01003 0 1e	4138.8770(3)	1.172269(4)	2.60(1)	0.21(1)
	01003 0 1f	4138.8772(4)	1.181742(5)	2.69(2)	-0.27(2)
N	01003 0 3e	4156.8634(5)	1.176154(6)	0.76(2)	-0.20(2)
N	01003 0 3f	4156.8638(6)	1.176148(7)	0.74(2)	0.27(2)

26/28	2554.9863(6)	$(4\nu_4+2\nu_5)^0$II - $(\nu_4+\nu_5)^0$	1.5	**P**
13/27	2666.7719(2)	$\nu_3 + \nu_4^1 - 2\nu_4^0$	1.0	**P**
70/78	2668.3601(2)	$\nu_3 + \nu_4^1 - 2\nu_4^2$	1.1	**P**
29/41	2666.7739(2)	$\nu_3 + \nu_4^1 - 2\nu_4^0$	1.0	**P**
49/94	2668.3621(2)	$\nu_3 + \nu_4^1 - 2\nu_4^2$	1.1	**P**
4/14	2565.6591(9)	$(4\nu_4+2\nu_5)^0$II - $(\nu_4+\nu_5)^0$	4.2	**P**
12/22	2677.7465(8)	$\nu_2+(2\nu_4+\nu_5)^1$I - $2\nu_4^0$	1.2	**P**
23/29	2677.7470(5)	$\nu_2+(2\nu_4+\nu_5)^1$I - $2\nu_4^0$	0.6	**P**
2/14	2679.7953(8)	$\nu_2+(2\nu_4+\nu_5)^3 - 2\nu_4^0$	0.4	**P**
15/15	2681.3834(8)	$\nu_2+(2\nu_4+\nu_5)^3 - 2\nu_4^2$	0.5	
5/8	2679.7968(8)	$\nu_2+(2\nu_4+\nu_5)^3 - 2\nu_4^0$	0.5	**P**
17/17	2681.3849(8)	$\nu_2+(2\nu_4+\nu_5)^3 - 2\nu_4^2$	0.7	
77/83	2626.0797(2)	$\nu_1 + \nu_4^1 - (\nu_4+\nu_5)^2$	0.6	
84/90	2640.8110(2)	$\nu_1 + \nu_4^1 - (\nu_4+\nu_5)^0$	1.0	
87/90	2626.0801(2)	$\nu_1 + \nu_4^1 - (\nu_4+\nu_5)^2$	0.9	
76/80	2628.3329(2)	$\nu_1 + \nu_4^1 - (\nu_4+\nu_5)^0$	0.9	
44/44	2658.4559(2)	$\nu_2+(\nu_4+2\nu_5)^1$II - $(\nu_4+\nu_5)^2$	1.0	
58/58	2660.7087(2)	$\nu_2+(\nu_4+2\nu_5)^1$II - $(\nu_4+\nu_5)^0$	0.8	
37/37	2658.4565(3)	$\nu_2+(\nu_4+2\nu_5)^1$II - $(\nu_4+\nu_5)^2$	0.8	
32/32	2673.1878(3)	$\nu_2+(\nu_4+2\nu_5)^1$II - $(\nu_4+\nu_5)^0$	0.4	
66/66	2672.7330(2)	$\nu_3 + \nu_5^1 - (\nu_4+\nu_5)^2$	0.6	
77/77	2687.4642(2)	$\nu_3 + \nu_5^1 - (\nu_4+\nu_5)^0$	0.6	
72/72	2672.7331(2)	$\nu_3 + \nu_5^1 - (\nu_4+\nu_5)^2$	0.6	
70/70	2674.9858(2)	$\nu_3 + \nu_5^1 - (\nu_4+\nu_5)^0$	0.6	
37/37	2696.3121(3)	$\nu_2+(\nu_4+2\nu_5)^1$I - $(\nu_4+\nu_5)^0$	0.5	
52/52	2696.3126(3)	$\nu_2+(\nu_4+2\nu_5)^1$I - $(\nu_4+\nu_5)^0$	0.6	
40/40	2689.9053(6)	$\nu_2+(\nu_4+2\nu_5)^3 - (\nu_4+\nu_5)^2$	0.7	
38/38	2689.9055(6)	$\nu_2+(\nu_4+2\nu_5)^3 - (\nu_4+\nu_5)^2$	0.5	
21/21	2862.3708(2)	$\nu_1 + \nu_5^1 - 2\nu_4^2$	1.0	
35/35	2642.0612(2)	$\nu_1 + \nu_5^1 - 2\nu_5^0$	0.6	
68/71	2632.8776(2)	$\nu_1 + \nu_5^1 - 2\nu_5^2$	0.9	
20/20	2862.3710(2)	$\nu_1 + \nu_5^1 - 2\nu_4^2$	1.0	
25/26	2642.0614(2)	$\nu_1 + \nu_5^1 - 2\nu_5^0$	0.9	
78/86	2632.8778(2)	$\nu_1 + \nu_5^1 - 2\nu_5^2$	0.8	
39/39	2689.7663(3)	$\nu_2 + 3\nu_5^1 - 2\nu_5^0$	0.6	
43/43	2680.5826(3)	$\nu_2 + 3\nu_5^1 - 2\nu_5^2$	0.8	
12/12	2689.7665(4)	$\nu_2 + 3\nu_5^1 - 2\nu_5^0$	0.6	
47/47	2680.5828(4)	$\nu_2 + 3\nu_5^1 - 2\nu_5^2$	0.8	
42/42	2698.5690(5)	$\nu_2 + 3\nu_5^3 - 2\nu_5^2$	0.7	
38/39	2698.5694(6)	$\nu_2 + 3\nu_5^3 - 2\nu_5^2$	0.4	

***P*=7**

	01031 3-1f	4486.1169(4)	1.175377(5)	2.24(1)		11/23	2631.5191(4)	$\nu_2+(3\nu_4+\nu_5)^2II - 3\nu_4^1$	1.3	P
						35/39	2634.7469(4)	$\nu_2+(3\nu_4+\nu_5)^2II - 3\nu_4^3$	1.2	P
	01031 3-1e	4486.1192(8)	1.17532(2)	17.5(1)	15.1(2)	11/24	2631.5214(8)	$\nu_2+(3\nu_4+\nu_5)^2II - 3\nu_4^1$	1.6	P
						20/39	2634.7492(8)	$\nu_2+(3\nu_4+\nu_5)^2II - 3\nu_4^3$	1.2	P
	01031 1-1e	4488.8383(5)	1.17533(2)	-14.5(2)	-20.0(6)	35/55	2634.2406(5)	$\nu_2+(3\nu_4+\nu_5)^0 - 3\nu_4^1$	1.3	P
	00120 2 0e	4504.5365(6)	1.17462(2)	12.1(1)	7.9(3)	22/25	2649.9387(6)	$\nu_3+2\nu_4^2 - 3\nu_4^1$	1.1	
						28/49	2653.1666(6)	$\nu_3+2\nu_4^2 - 3\nu_4^3$	0.9	P
	00120 2 0f	4504.5381(5)	1.17451(2)	1.5(1)	-1.8(3)	21/29	2649.9411(5)	$\nu_3+2\nu_4^2 - 3\nu_4^1$	1.0	P
						32/45	2653.1632(5)	$\nu_3+2\nu_4^2 - 3\nu_4^3$	0.8	P
	00120 0 0e	4508.0123(5)	1.17501(3)	-8.4(3)	-12(1)	28/53	2653.4145(5)	$\nu_3+2\nu_4^0 - 3\nu_4^1$	0.9	P
N	10020 0 0e	4569.4659(5)	1.17347(2)	23.4(1)	31.8(4)	24/39	2609.7742(5)	$\nu_1 + 2\nu_4^0 - (2\nu_4+\nu_5)^1I$	2.0	P
						30/47	2629.4660(5)	$\nu_1 + 2\nu_4^0 - (2\nu_4+\nu_5)^1II$	2.0	P
N	10020 2 0e	4570.6925(5)	1.17282(2)	-21.3(2)	-36.6(6)	3/7	2611.0008(5)	$\nu_1 + 2\nu_4^2 - (2\nu_4+\nu_5)^1I$	4.0	
						23/38	2608.7593(5)	$\nu_1 + 2\nu_4^2 - (2\nu_4+\nu_5)^3$	1.0	P
						18/25	2630.6926(5)	$\nu_1 + 2\nu_4^2 - (2\nu_4+\nu_5)^1II$	1.8	P
N	10020 2 0f	4570.6954(3)	1.172748(3)	1.711(5)		6/7	2611.0037(3)	$\nu_1 + 2\nu_4^2 - (2\nu_4+\nu_5)^1I$	1.4	
						41/41	2608.7622(3)	$\nu_1 + 2\nu_4^2 - (2\nu_4+\nu_5)^3$	0.7	
						40/40	2630.6955(3)	$\nu_1 + 2\nu_4^2 - (2\nu_4+\nu_5)^1II$	1.0	
N	01022 2-2e	4590.0810(8)	1.175596(9)			6/11	2630.3893(8)	$\nu_2+(2\nu_4+2\nu_5)^0II - (2\nu_4+\nu_5)^1I$	2.2	P
	01022 2-2f	4599.7738(7)	1.17652(3)	5.8(3)	13.1(8)	13/37	2640.0817(7)	$\nu_2+(2\nu_4+2\nu_5)^0II - (2\nu_4+\nu_5)^1I$	2.0	P
	01022 2 0e	4603.2303(6)	1.176554(3)			6/10	2643.5386(6)	$\nu_2+(2\nu_4+2\nu_5)^2II - (2\nu_4+\nu_5)^1I$	2.3	P
						2/4	2641.2982(6)	$\nu_2+(2\nu_4+2\nu_5)^2II - (2\nu_4+\nu_5)^3$	0.5	P
	01022 2 0f	4603.290(2)	1.17559(3)	0.51(8)		4/13	2643.599(2)	$\nu_2+(2\nu_4+2\nu_5)^2II - (2\nu_4+\nu_5)^1I$	0.7	P
						2/4	2641.358(2)	$\nu_2+(2\nu_4+2\nu_5)^2II - (2\nu_4+\nu_5)^3$	0.9	P
	00111 1-1e	4609.3393(5)	1.175539(8)	5.04(3)	1.05(3)	39/39	2669.3394(5)	$\nu_3+(\nu_4+\nu_5)^0 - (2\nu_4+\nu_5)^1II$	1.2	
	00111 1-1f	4617.9258(3)	1.175544(6)	2.03(3)	-0.70(3)	36/36	2658.2337(3)	$\nu_3+(\nu_4+\nu_5)^0 - (2\nu_4+\nu_5)^1I$	1.1	
						26/26	2677.9271(3)	$\nu_3+(\nu_4+\nu_5)^0 - (2\nu_4+\nu_5)^1II$	1.7	P
	00111 1 1f	4620.0544(4)	1.175011(3)	1.703(6)		26/26	2660.3628(4)	$\nu_3+(\nu_4+\nu_5)^2 - (2\nu_4+\nu_5)^1I$	1.6	
						22/22	2658.1213(4)	$\nu_3+(\nu_4+\nu_5)^2 - (2\nu_4+\nu_5)^3$	0.9	
	00111 1 1e	4620.0557(5)	1.174964(8)	-1.57(3)	-0.68(3)	26/26	2660.3641(5)	$\nu_3+(\nu_4+\nu_5)^2 - (2\nu_4+\nu_5)^1I$	1.6	
						24/24	2658.1226(5)	$\nu_3+(\nu_4+\nu_5)^2 - (2\nu_4+\nu_5)^3$	0.9	
N	02001 0 1f	4659.795(1)	1.168082(8)			3/3	2685.472(1)	$2\nu_2+\nu_5^1 - \nu_2$	1.6	
N	02001 0 1e	4659.801(2)	1.16341(2)			3/3	2685.478(2)	$2\nu_2+\nu_5^1 - \nu_2$	2.0	
	10011 1-1e	4673.6307(3)	1.174062(5)	3.79(2)	0.29(2)	55/60	2625.7542(3)	$\nu_1+(\nu_4+\nu_5)^0 - (\nu_4+2\nu_5)^1II$	0.8	
	10011 1 1e	4687.3616(3)	1.173497(3)	-0.146(6)		24/25	2639.4852(3)	$\nu_1+(\nu_4+\nu_5)^2 - (\nu_4+2\nu_5)^1II$	1.5	
						7/7	2621.5678(3)	$\nu_1+(\nu_4+\nu_5)^2 - (\nu_4+2\nu_5)^1I$	1.6	
						40/47	2613.1826(3)	$\nu_1+(\nu_4+\nu_5)^2 - (\nu_4+2\nu_5)^3$	1.0	
	10011 1 1f	4687.3629(2)	1.173471(2)	1.738(3)		24/24	2639.4865(2)	$\nu_1+(\nu_4+\nu_5)^2 - (\nu_4+2\nu_5)^1II$	0.9	

						7/7	2621.5691(3)	$\nu_1+(\nu_4+\nu_5)^2$ - $(\nu_4+2\nu_5)^1$I	1.6
						50/52	2613.1839(2)	$\nu_1+(\nu_4+\nu_5)^2$ - $(\nu_4+2\nu_5)^3$	1.2
	10011 1-1f	4688.8394(3)	1.173380(2)	1.627(3)		54/55	2623.0456(3)	$\nu_1+(\nu_4+\nu_5)^0$ - $(\nu_4+2\nu_5)^1$I	1.1
	01013 1-1e	4710.735(1)	1.17764(2)	6.59(5)		6/6	2644.942(1)	$\nu_2+(\nu_4+3\nu_5)^0$ - $(\nu_4+2\nu_5)^1$I	0.5
	00102 0 0e	4727.0684(6)	1.17627(1)	5.44(6)	1.02(7)	18/20	2679.1918(6)	$\nu_3+2\nu_5^0$ - $(\nu_4+2\nu_5)^1$II	0.9
						16/16	2661.2767(6)	$\nu_3+2\nu_5^0$ - $(\nu_4+2\nu_5)^1$I	1.1
	00102 0 2e	4736.3131(4)	1.176002(6)	-2.04(2)		9/9	2688.4374(4)	$\nu_3+2\nu_5^2$ - $(\nu_4+2\nu_5)^1$II	1.6
						9/9	2662.1341(4)	$\nu_3+2\nu_5^2$ - $(\nu_4+2\nu_5)^3$	1.8
						9/9	2670.5215(4)	$\nu_3+2\nu_5^2$ - $(\nu_4+2\nu_5)^1$I	1.4
	00102 0 2f	4736.3141(6)	1.17598(1)	1.89(5)		9/9	2688.4384(6)	$\nu_3+2\nu_5^2$ - $(\nu_4+2\nu_5)^1$II	1.4
						7/7	2662.1351(6)	$\nu_3+2\nu_5^2$ - $(\nu_4+2\nu_5)^3$	1.8
						7/7	2670.5225(6)	$\nu_3+2\nu_5^2$ - $(\nu_4+2\nu_5)^1$I	1.8
N	01013 1-1f	4740.210(1)	1.17705(1)			2/3	2674.418(1)	$\nu_2+(\nu_4+3\nu_5)^0$ - $(\nu_4+2\nu_5)^1$I	0.0
	10002 0 0e	4800.1351(4)	1.174525(7)	4.46(3)	0.64(3)	51/51	2630.9776(4)	$\nu_1 + 2\nu_5^0$ - $3\nu_5^1$	0.9
	10002 0 2f	4809.5098(5)	1.174023(7)	1.77(3)	0.15(3)	13/13	2640.3523(5)	$\nu_1 + 2\nu_5^2$ - $3\nu_5^1$	1.2
						30/30	2622.0592(5)	$\nu_1 + 2\nu_5^2$ - $3\nu_5^3$	0.8
	1000202e	4809.5104(5)	1.173977(8)	-1.06(4)	-0.61(5)	18/19	2640.3529(5)	$\nu_1 + 2\nu_5^2$ - $3\nu_5^1$	1.4
						32/32	2622.0598(5)	$\nu_1 + 2\nu_5^2$ - $3\nu_5^3$	0.9

Notes

The confidence interval (1 SD) is given in parenthesis in the unit of the last quoted digit. The parameters of the lower vibrational levels of $^{12}C_2H_2$ were constrained to the values given in Refs. [12,13].

[a]Normal mode labeling: $V_{i=1-5}$ are the vibrational quantum numbers, $\ell_{4,5}$ are the vibrational angular momentum quantum numbers associated to the degenerate bending modes and ε=e or f is the symmetry type relative to the Wang transformation. The labeling was obtained according to the maximum value of the modulus squared of the expansion coefficients of the vibrational eigenfunction in the normal mode basis (for low J values). "N" marks upper states newly observed.

[b]N_{tot} is the total number of the observed transitions reaching a given vibrational state and n_{fit} is the number of positions included in the fit of the parameters.

[c] Band center: $\Delta G_c = G_c^{'} - G_c^{''}$

[d] Observed band in Plíva notation [15].

[e]Root mean square deviation in 10^{-3} cm^{-1} unit. "P" marks perturbed states.

[f]The spectroscopic constants of the ν_2 state have been obtained fitting the ν_2-ν_5 band from Ref. [14].

In Ref. [1] the recommended line list was constructed as a mix of measurements and calculations and no interpolations was performed where large deviations were observed. In the present work we found a more accurate way to generate line positions using a mix of calculations from spectroscopic constants and predictions (most of the time rescaled) from the effective Hamiltonian (ASD-1000). The rescaling of the EH predictions allows, in most cases, better agreement with the measurements than the calculations using spectroscopic constants. The main advantage of the EH predictions is that most of the interactions are taken into account so that, contrary to the calculation with spectroscopic constants, no drastic deviation from measurements is observed in cases of perturbation.

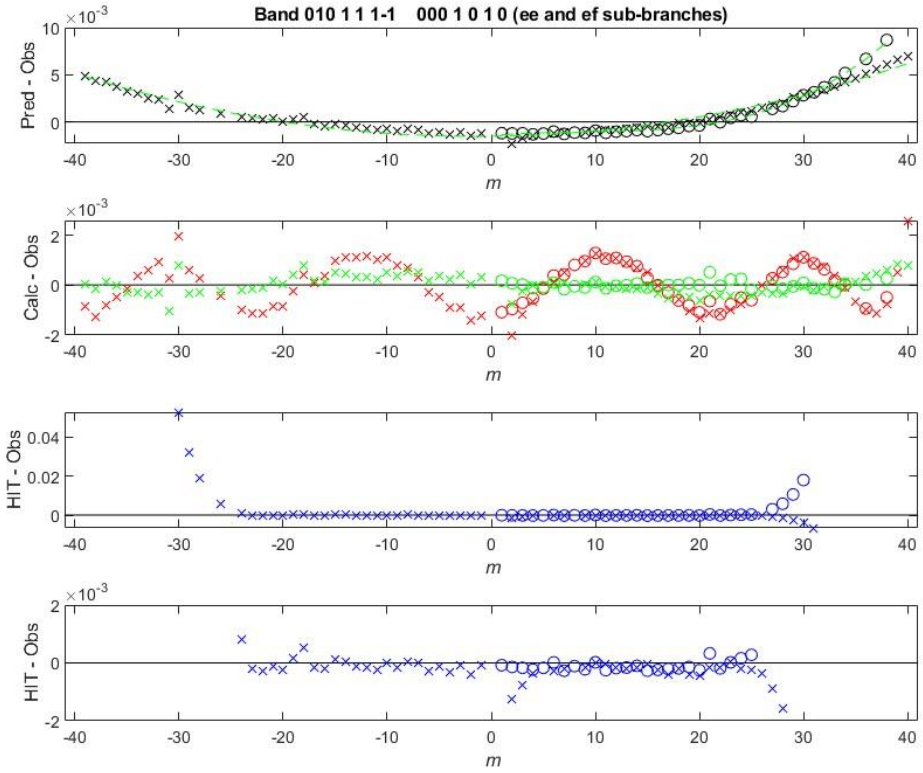

Fig.2. Residuals in cm^{-1} obtained for the $\nu_2+(\nu_4+\nu_5)^0$ - ν_4^1 band present in HITRAN and GEISA databases. Cross symbols are used for the P_{ee} and R_{ee} branches and open circles for the Q_{ef} branch. See text for details.

A first example is given in Fig. 2 for the P_{ee}, Q_{ef} and R_{ee} sub-branches of the $\nu_2+(\nu_4+\nu_5)^0$ - ν_4^1 band included in the HITRAN and GEISA databases. Note that the $\nu_2+(\nu_4+\nu_5)^0$ - ν_4^1 band contains also the weaker P_{ff}, Q_{fe} and R_{ff} sub-branches that have been measured for the first time in the present work. In Fig. 2, first panel presents residuals in cm^{-1} between predictions with effective Hamiltonian and measurements

(cross symbols for P_{ee} and R_{ee} sub-branches and open circles for Q_{ef} sub-branch for all panels of Fig. 2). As it can be observed the residuals smoothly increase from -2×10^{-3} cm^{-1} for lowest *m* values up to 5×10^{-3} cm^{-1} for highest *m* values in the *P* branch, and up to 7×10^{-3} and $9\times10^{-3}cm^{-1}$ for highest *m* values in the *R* and *Q* branches respectively (*m* is -*J*, *J* and *J*+1 in *P*, *Q* and *R* branches, respectively). These smooth residuals can be easily modeled using polynomial expressions of the order 2-4 depending on branches (dashed-green line in the upper panel of Fig. 2). The subtraction of the fitted polynomial values from the EH predictions allows rich satisfactory modelling of the line positions. Note that polynomial modelling of the residuals in the *Q* branch differs from that for *P* and *R* branches. In the second panel of Fig. 2 the residuals obtained with the rescaled EH predictions (green symbols) are plotted together with the residuals obtained using spectroscopic constants of the Table 1(red symbols). As it can be observed in the second panel, the oscillations in red residuals are much larger comparing to the green ones, implying the use for this band of the rescaled EH predictions instead of spectroscopic constants calculations. In the last two panels the residuals between HITRAN and measured line positions are given (blue symbols). In the last panel the vertical scale is reduced to +/- 0.002 cm^{-1}. It can be clearly observed that the residuals are very good in the range of measurements of Ref. [2] but increase quickly from *J* = 25 pointing out the limitations of the extrapolate calculations based on spectroscopic constants as it was performed in Ref. [2]. The deviation between databases and measurements in the cases of such extrapolations can reach several cm^{-1} as for the *Q*-branch of the ν_3 - ν_4^1 band presented in Fig. 3 (see third panel). Once again, the rescaled predictions (green symbols) give better agreement with the measurements then the spectroscopic constants (red symbols). Note that the same symbols have been used in Figs. 2-6.

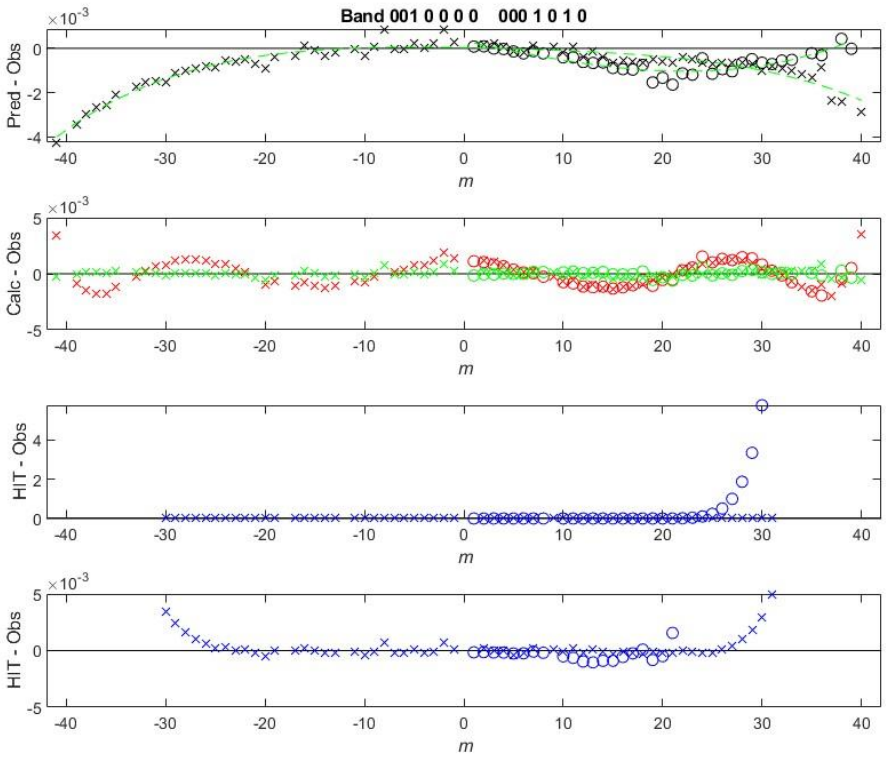

Fig.3. Residuals in cm^{-1} obtained for the ν_3 - ν_4^1 band present in HITRAN and GEISA databases. Cross symbols are used for the P_{ee} and R_{ee} branches and open circles for the Q_{ef} branch. See text for details.

Fig. 4 shows the residuals obtained for the $\nu_2+(\nu_4+\nu_5)^0$ - ν_4^1 sub-band absent in HITRAN and GEISA databases. The residuals for P_{ff} and R_{ff} branches are given by plus symbols and those for Q_{fe} branch by dot symbols. As it can be seen the both residuals (with spectroscopic constants calculations or with rescaled EH predictions) are similar and within +/- 0.0005 cm^{-1}. In such case the calculations with spectroscopic constants from Table 1 have been used for final recommended line list.

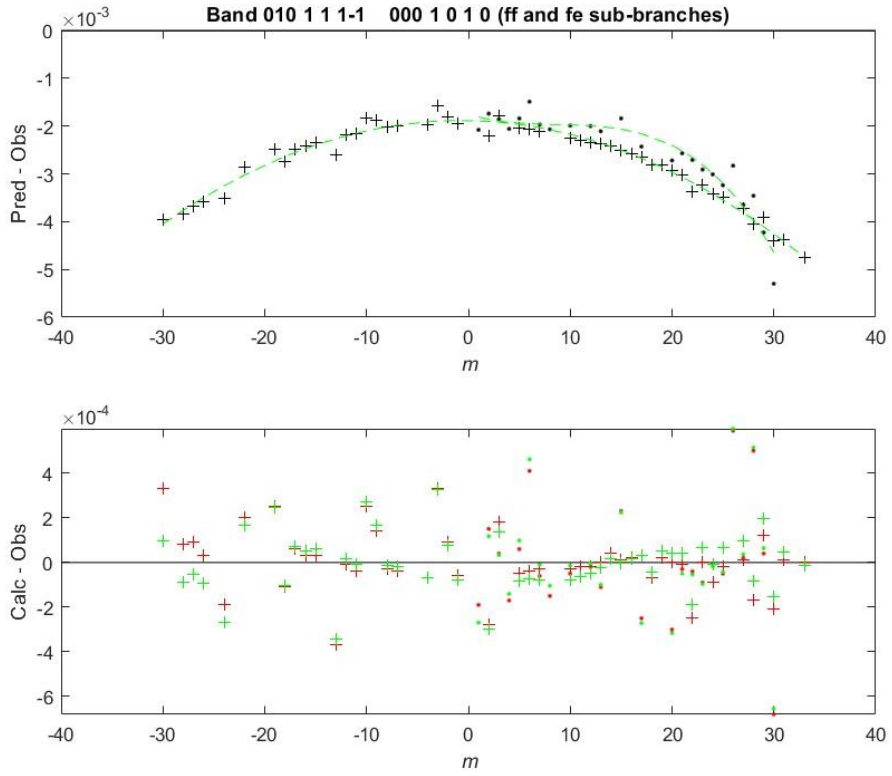

Fig.4. Residuals in cm^{-1} obtained for the $\nu_2+(\nu_4+\nu_5)^0$ - ν_4^1 *ff* and *fe* sub-band observed for the first time. For the P_{ff} and R_{ff} branches the symbol plus is used while the point is used for Q_{fe} branch. See text for details.

In Fig. 5, the residuals are plotted for the $\nu_2+2\nu_5^0$ - ν_5^1 band demonstrating the improvement of the residuals using rescaled predictions (green symbols) comparing to the spectroscopic constants calculations (red symbols). In Fig. 6 the calculations with spectroscopic constants show drastic increases of the residuals for high *m* values (red symbols) while the rescaled predictions (green symbols) accurately describes the line positions of the $\nu_3+2\nu_4^0$ - $3\nu_4^1$ band.

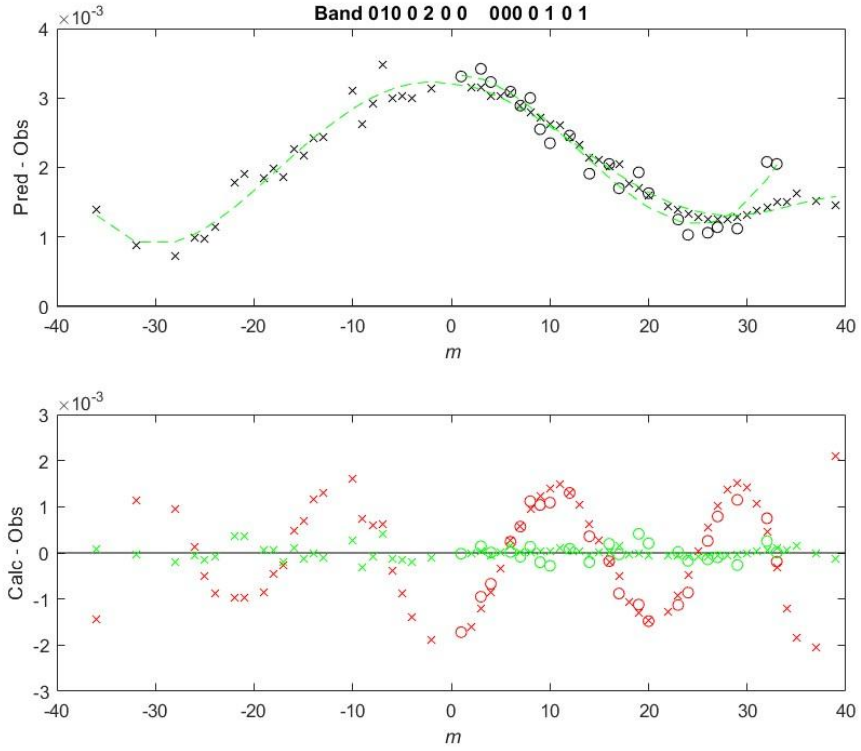

Fig.5. Residuals in cm^{-1} obtained for the $\nu_2+2\nu_5^0 - \nu_5^1$ band observed for the first time. Cross symbols are used for the P_{ee} and R_{ee} branches and open circles for the Q_{ef} branch. See text for details.

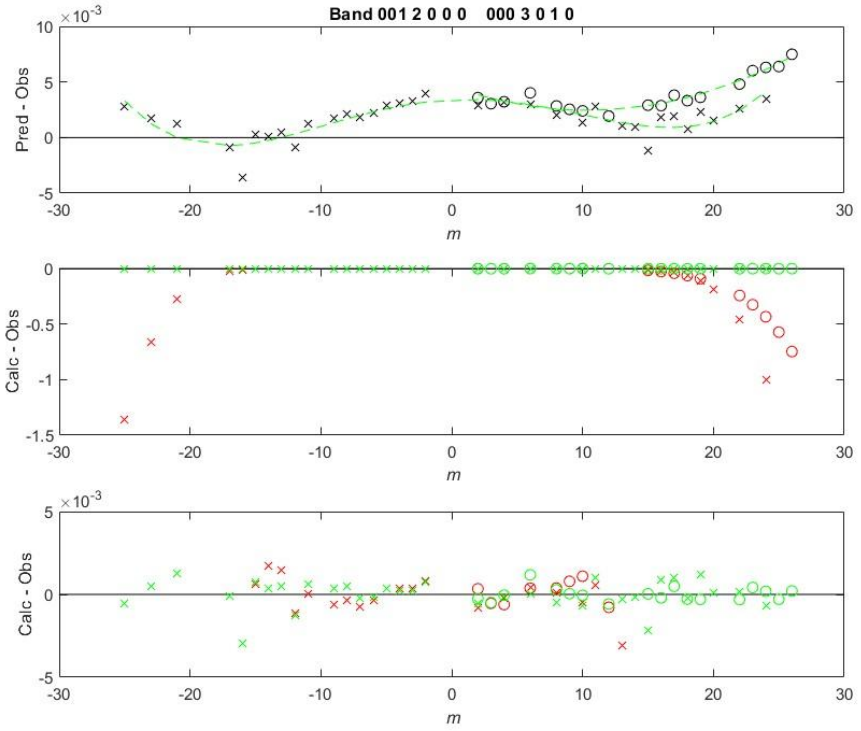

Fig.6. Residuals in cm^{-1} obtained for the $\nu_3+2\nu_4^0 - 3\nu_4^1$ band observed for the first time. Cross symbols are used for the P_{ee} and R_{ee} branches and open circles for the Q_{ef} branch. See text for details.

5. Effective dipole moment fitting and comparisons with measurements

The effective dipole moment parameters reported in Ref. [3] were obtained by the fitting of the line intensities of five vibrational bands [2] with the maximum J values around 20-25. In the present work measurements for these five bands were greatly extended up to J = 39-43 depending on the band while the measurements for low J values were not performed. The new measurements allowed refine the set of EDM parameters. The definition of the parameters and the calculation formulas can be found in Refs. [3,5,16]. The line intensity fit including all available measurements (this work and Ref. [1,2]) for 71 bands was performed. The statistical information on the result of the fit is collected in Table 2. The result of fit of the bands measured in Ref. [1] and in this work is slightly worse with RMS about 3-5% comparing to 1-2% for the strongest bands measured in Ref. [2]. The larger deviations can be explained by the weakness of the measured lines but also by the fact that many transitions are overlapped due to long optical absorption paths used in Ref. [1] and present work.

Table 2. Band statistics of the EDM parameters fit in the 3.8-μm spectral region.

Upper level - Lower level ($V_1V_2V_3V_4V_5\ell_4\ell_5$)	Region (cm^{-1})	J_{max}	N	MR(%)	RMS(%)
Bands present in the 2020 edition of the HITRAN and GEISA databases. Statistics are presented twice for each band, first corresponding to the EDM fit using measurements from Ref. [2], and then using measurements of this work.					
0 1 0 0 1 0 1 - 0 0 0 0 0 0 0 0	2649.8-2752.4	25	60	0.77	1.40
	2601.0-2792.1	43	42	-2.60	3.95
0 0 0 3 1 1-1 - 0 0 0 0 0 0 0 0	2515.5-2609.0	21	33	1.16	2.11
	2491.3-2647.1	35	26	-1.12	3.53
1 0 0 0 0 0 0 - 0 0 0 0 1 0 1	2583.7-2694.1	24	55	-0.18	0.86
	2534.0-2728.3	42	34	0.72	1.95
0 1 0 1 1 1-1 - 0 0 0 1 0 1 0	2627.3-2737.2	24	57	0.39	0.85
	2585.2-2769.3	39	94	0.65	2.71
0 0 1 0 0 0 0 - 0 0 0 1 0 1 0	2614.6-2713.7	23	39	-0.36	1.95
	2573.5-2757.7	39	45	0.49	3.16
Bands measured for the first time in the present work					
0 0 0 1 3 1-1 - 0 0 0 0 0 0 0 0	2728.4-2807.3	19	23	0.15	3.11
0 0 0 3 1 1 1 - 0 0 0 0 0 0 0 0	2541.7-2623.8	19	3	-2.24	6.14
0 0 0 4 1 4-1 - 0 0 0 1 0 1 0	2501.8-2635.5	29	25	1.57	4.46
0 0 0 5 1 1-1 - 0 0 0 2 0 0 0	2539.1-2634.0	23	23	-0.79	4.06
0 0 0 5 1 3-1 - 0 0 0 2 0 2 0	2533.9-2639.3	24	44	-0.28	3.60
0 0 1 0 2 0 0 - 0 0 0 1 2 1 0	2638.5-2720.7	17	1	5.83	5.83
0 0 1 0 2 0 0 - 0 0 0 1 2-1 2	2634.3-2661.1	11	3	-5.48	5.80
0 0 1 0 2 0 2 - 0 0 0 1 2 1 0	2688.1-2716.5	13	6	-2.19	4.62
0 0 1 0 2 0 2 - 0 0 0 1 2 1 2	2635.6-2655.0	5	2	0.94	7.08
0 0 1 0 2 0 2 - 0 0 0 1 2-1 2	2668.5-2697.7	15	5	1.99	6.14
0 0 1 1 1 1 1 - 0 0 0 2 1 0 1	2609.1-2714.3	23	12	-2.92	4.51
0 0 1 1 1 1 1 - 0 0 0 2 1 2 1	2621.4-2696.6	22	20	0.33	4.60

0 0 1 1 1 1-1 – 0 0 0 2 1 0 1	2617.0-2685.9	22	14	1.92	4.57
0 0 1 1 1 1-1 – 0 0 0 2 1 2-1	2626.1-2712.8	22	24	-0.26	4.90
0 0 1 2 0 0 0 – 0 0 0 3 0 1 0	2593.5-2704.7	26	30	1.71	4.57
0 0 1 2 0 2 0 – 0 0 0 3 0 1 0	2613.7-2686.2	27	23	-3.24	6.40
0 0 1 2 0 2 0 – 0 0 0 3 0 3 0	2581.3-2710.5	29	43	1.29	4.31
0 1 0 0 2 0 0 – 0 0 0 0 1 0 1	2601.8-2775.9	38	62	0.80	3.91
0 1 0 0 2 0 2 – 0 0 0 0 1 0 1	2637.3-2776.1	35	128	-0.04	3.04
0 1 0 0 3 0 1 – 0 0 0 0 2 0 0	2626.1-2749.3	27	33	0.40	3.46
0 1 0 0 3 0 1 – 0 0 0 0 2 0 2	2647.7-2744.3	26	27	-0.15	4.36
0 1 0 0 3 0 3 – 0 0 0 0 2 0 2	2652.0-2756.1	28	42	-0.09	4.50
0 1 0 1 1 1 1 – 0 0 0 1 0 1 0	2636.2-2764.9	36	91	-0.92	3.17
0 1 0 1 2 1 2 – 0 0 0 1 1 1 1	2651.0-2744.0	23	38	-0.25	4.04
0 1 0 1 2-1 2 – 0 0 0 1 1 1-1	2626.4-2744.6	27	50	1.67	3.94
0 1 0 2 1 0 1 – 0 0 0 2 0 0 0	2630.4-2717.9	19	28	-0.52	3.79
0 1 0 2 1 2 1 – 0 0 0 2 0 0 0	2637.6-2715.7	23	6	-2.04	3.91
0 1 0 2 1 2 1 – 0 0 0 2 0 2 0	2657.4-2715.8	19	15	0.58	3.56
0 1 0 2 2 2 0 – 0 0 0 2 1 0 1	2668.8-2668.8	0	0	0.00	0.00
0 1 0 2 2 2-2 – 0 0 0 2 1 0 1	2604.0-2637.8	20	7	-4.57	6.60
0 1 0 3 1 1-1 – 0 0 0 3 0 1 0	2580.0-2681.6	26	24	-0.35	4.75
0 1 0 3 1 3-1 – 0 0 0 3 0 1 0	2610.2-2647.9	21	6	-0.89	5.39
0 1 0 3 1 3-1 – 0 0 0 3 0 3 0	2571.3-2687.8	26	35	0.12	4.37
1 0 0 0 1 0 1 – 0 0 0 2 0 2 0	2823.5-2887.7	16	13	0.49	5.38
1 0 0 0 2 0 0 – 0 0 0 0 3 0 1	2566.5-2671.7	24	19	-1.57	4.76
1 0 0 0 2 0 2 – 0 0 0 0 3 0 1	2606.6-2656.6	21	5	-1.08	5.37
1 0 0 0 2 0 2 – 0 0 0 0 3 0 3	2566.5-2664.0	24	30	-0.16	5.02
1 0 0 1 1 1 1 – 0 0 0 1 2 1 0	2592.6-2663.8	20	16	-2.26	5.32
1 0 0 1 1 1-1 – 0 0 0 1 2-1 2	2568.1-2622.7	23	14	-4.36	6.07
1 0 0 2 0 0 0 – 0 0 0 2 1 0 1	2557.7-2646.1	23	19	-4.14	6.10
1 0 0 2 0 0 0 – 0 0 0 2 1 2-1	2562.9-2675.0	26	31	-3.52	5.55
1 0 0 2 0 2 0 – 0 0 0 2 1 0 1	2576.7-2610.3	20	3	-1.59	4.01
1 0 0 2 0 2 0 – 0 0 0 2 1 2 1	2549.4-2656.1	24	57	-0.45	4.01
1 0 0 2 0 2 0 – 0 0 0 2 1 2-1	2575.8-2646.9	21	21	-0.16	6.02
0 0 1 0 1 0 1 – 0 0 0 1 1 1 1	2607.6-2741.1	30	100	-0.33	3.67
0 0 1 0 1 0 1 – 0 0 0 1 1 1-1	2607.2-2748.2	31	96	0.94	3.07
0 1 0 2 1 2-1 – 0 0 0 2 0 0 0	2601.7-2685.5	31	32	-4.30	5.93
0 1 0 2 1 2-1 – 0 0 0 2 0 2 0	2565.2-2726.7	35	99	-0.01	3.32
0 1 0 1 2 1 0 – 0 0 0 1 1 1 1	2607.7-2695.8	21	31	-1.50	6.02
0 1 0 1 2 1 0 – 0 0 0 1 1 1-1	2595.7-2733.6	31	54	-0.15	4.01
0 0 1 1 0 1 0 – 0 0 0 2 0 0 0	2611.8-2715.7	33	37	-2.23	4.59
0 0 1 1 0 1 0 – 0 0 0 2 0 2 0	2580.7-2745.9	35	119	0.10	3.78
Bands previously measured in Ref. [1]					
0 0 0 3 1 3-1 – 0 0 0 0 0 0 0	2469.6-2636.4	37	41	1.60	3.11
0 0 0 3 2 3 0 – 0 0 0 0 1 0 1	2493.1-2603.9	25	25	-1.34	4.83
0 0 0 3 2 3-2 – 0 0 0 0 1 0 1	2458.1-2596.5	27	61	-0.21	3.79
0 0 0 3 2-1 2 – 0 0 0 0 1 0 1	2490.5-2606.1	28	66	-1.52	3.36
0 0 0 4 1 2-1 – 0 0 0 1 0 1 0	2507.5-2652.5	32	71	0.48	2.43
0 0 0 4 2 2-2 – 0 0 0 1 1 1-1	2511.8-2587.2	20	18	1.28	3.89
0 1 0 2 0 0 0 – 0 0 0 0 1 0 1	2399.8-2498.4	29	47	1.18	4.00
0 1 0 2 0 2 0 – 0 0 0 0 1 0 1	2389.1-2514.5	30	39	-0.99	5.29
1 0 0 0 1 0 1 – 0 0 0 0 2 0 0	2557.5-2705.5	32	33	0.19	3.18
1 0 0 0 1 0 1 – 0 0 0 0 2 0 2	2545.7-2691.7	34	70	1.85	3.64
1 0 0 1 0 1 0 – 0 0 0 1 1 1 1	2547.7-2695.2	32	71	1.99	4.00
1 0 0 1 0 1 0 – 0 0 0 1 1 1-1	2549.8-2707.1	34	77	-1.32	4.13
1 0 0 1 1 1 1 – 0 0 0 1 2 1 2	2560.4-2612.7	21	24	1.76	4.77
1 0 0 1 1 1-1 – 0 0 0 1 2 1 0	2564.2-2670.9	25	13	-0.30	3.56

Note: for a given band, J_{max} is the maximum observed value of the rotational quantum number of the lower state, N is the number of the measured line intensities included in the fit. *MR* and *RMS* are the mean value and the root mean square of the residuals, respectively. Its definition can be found for example in Ref. [3].

The effective dipole moment parameters obtained by the fitting of the present line intensities together with those from Refs. [1,2] (using formulas of Ref. [5,16]) are collected in the Table 3. The parameters obtained in Refs. [1,3] are also presented. In the Ref. [1] the satisfactory description of the line intensities of all 19 bands was achieved by adding only three small parameters to the set of Ref. [3]. In this work an accurate description of all 71 bands was obtained by adding 9 supplemental parameters to the set of Ref. [1].

Table 3. The set of the effective dipole moment parameters describing the line intensities of acetylene in the 3.8-μm spectral region

Parameter[a]	ΔV_1	ΔV_2	ΔV_3	ΔV_4	ΔV_5	$\Delta \ell_4$	$\Delta \ell_5$	PW[b]	[1][b]	[3][b]	Order
M	0	1	0	0	1	0	1	-0.2359(3)	-0.2401(4)	-0.2377(2)	10^{-2}
k_4	0	1	0	0	1	0	1	-0.089(1)	-0.183(7)	-0.191(4)	
b_J	0	1	0	0	1	0	1	0.589(5)	0.55(1)	0.557(8)	10^{-2}
k_5	0	1	0	0	1	0	1	-0.080(1)			
a_5	0	1	0	0	1	0	1	0.0132(5)			
M	1	0	0	0	-1	0	1	-1.1642(8)	-1.168(1)	1.121(1)	10^{-2}
b_J	1	0	0	0	-1	0	1	-0.364(5)	-0.353(6)	-0.398(8)	10^{-2}
M	0	0	1	-1	0	1	0	1.063(2)	1.047(1)	1.0360(7)	10^{-2}
b_J	0	0	1	-1	0	1	0	-0.357(4)	-0.36(1)	-0.361(6)	10^{-2}
k_4	0	0	1	-1	0	1	0	-1.56(8)			10^{-2}
k_5	0	0	1	-1	0	1	0	-2.2(1)			10^{-2}
M	0	0	0	1	3	1	-1	3.094(9)			10^{-5}
b_J	0	0	0	1	3	1	-1	-1.14(2)			10^{-2}
M	0	0	0	3	1	1	-1	1.609(2)	1.631(2)	1.621(2)	10^{-4}
k_4	0	0	0	3	1	1	-1	-0.032(1)	-0.027(2)		
M	0	1	0	2	-1	0	1	1.597(6)	1.630(7)		10^{-4}
M	0	1	0	2	-1	2	-1	0.959(4)	0.934(4)		10^{-4}
M	1	0	0	-2	1	2	-1	-0.61(3)			10^{-4}
M	0	1	0	0	1	2	-1	1.38(2)			10^{-4}
M	0	0	1	-1	0	-1	2	-1.08(6)			10^{-4}

[a] Parameters M are given in Debye (1 D = 3.33546×10^{-30} C·m), while the other parameters are dimensionless.
[b] Confidence intervals (1 SD, in unit of the last quoted digit) are given between parenthesis.

The vibration-rotation transition moment squared $|R|^2$ calculated using Eq. (2) of Ref. [1] has usually smooth rotational dependence and is useful to analyze the measured intensities. For each band measured and calculated $|R|^2$ were plotted versus m (m = -J, J,

J+1 for *P*, *Q* and *R* branches respectively). Such plots have been used to check the quality of the intensities calculation. Examples are given in Figs. 7 and 8 respectively for the two bands ν_3-ν_4^1 and $(3\nu_4+\nu_5)^0$, present in the 2020 edition of the HITRAN and GEISA databases. In these figures we can first observe the good consistency between measurements from this work and those from Ref. [2], with a dispersion of the measurements slightly higher for this work. Note that under present experimental conditions, only transitions with high *J* values could be measured with sufficient accuracy, transitions with lower *J* values are saturated in all experimental spectra of this work. In Figs. 7 and 8, one can see that the calculations using EDM parameters from this work (red line) and from previous study [1] (blue line) are very similar since these bands were already included in the fit of EDM parameters in the previous work [3]. It is worth to notice that EDM calculation from Ref. [1] predicts accurately the rotational dependence observed for high *J* values measured for the first time in this work. The calculation in HITRAN and GEISA databases (using Herman-Wallis factor to fit observed rotational dependences from measurements of Ref. [2]) is also quite close to calculations using EDM parameters. Note that extrapolations of the measurements from the Ref. [2] have been performed for the databases using fixed value of the transition dipole moment squared leading to the singularities in its rotational dependence.

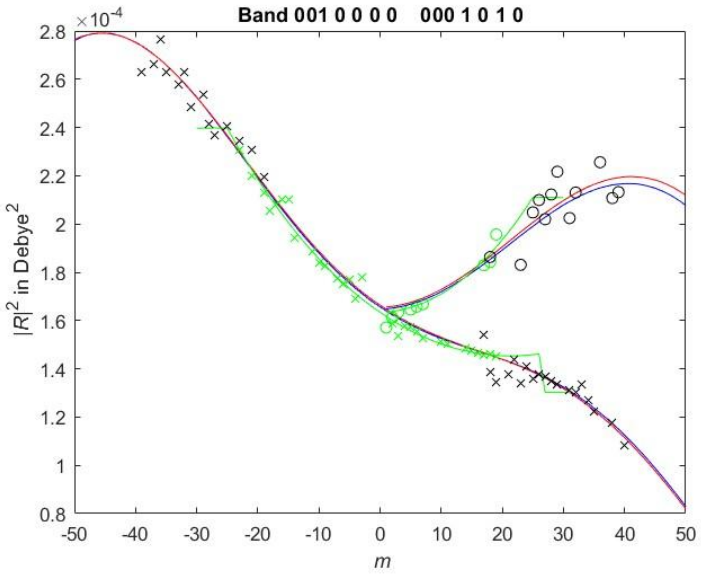

Fig.7. Vibration-rotation transition moments squared $|R|^2$ obtained for the ν_3 - ν_4^1 band. Cross symbols for P_{ee} and R_{ee} sub-branches and open circles symbols for Q_{ef} sub-branch have been used for measurements from this work (black symbols) and from Ref. [2] (green symbols). Continuous lines correspond to calculations: red and blue lines stand for calculations with EDM parameters from this work and from Ref. [1] respectively, whereas green line stands for the calculation given in the HITRAN and GEISA databases.

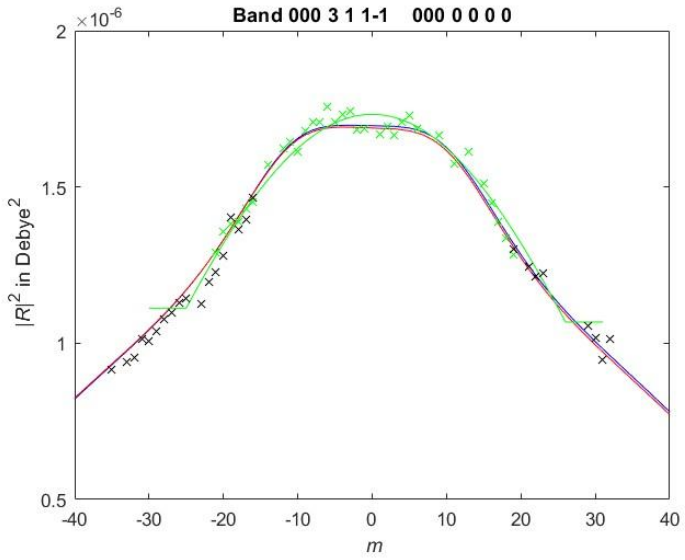

Fig.8. Vibration-rotation transition moments squared $|R|^2$ obtained for the $(3\nu_4+\nu_5)^0$ band. See Fig. 7 for legend.

Transition dipole moment squared belonging to the $(\nu_4+3\nu_5)^0$, $\nu_2+2\nu_5{}^0$ - $\nu_5{}^1$ and $\nu_3+\nu_4{}^1$ - $2\nu_4{}^0$ bands (newly observed) have been plotted in Figs. 9-11 respectively together with calculations using EDM parameters (see Table 3) from Ref. [1] (blue line) and from this work (red line). As it can be observed in Figs. 9-11, except the cold band the rotational dependence of $|R|^2$ values predicted by EDM parameters of Ref. [1] is in good agreement with the measurements obtained for the first time in this work. Two additional EDM parameters were required (principal "*M"* and rotational dependence "b_J" parameters, see Table 3) to describe the intensities in the cold $(\nu_4+3\nu_5)^0$ band presented in Fig. 9. The vibrational transition moment squared of hot bands was slightly corrected by new set of parameters. Since the EDM model takes into account resonance interactions between levels, it allows to reach a good qualitative rotational dependence where intensity modelling using Herman-Wallis factors fails. We believe that using EDM parameters extrapolations of intensities could be performed without risking hazardous extrapolations. This is certainly not the case of model using Herman-Wallis factors.

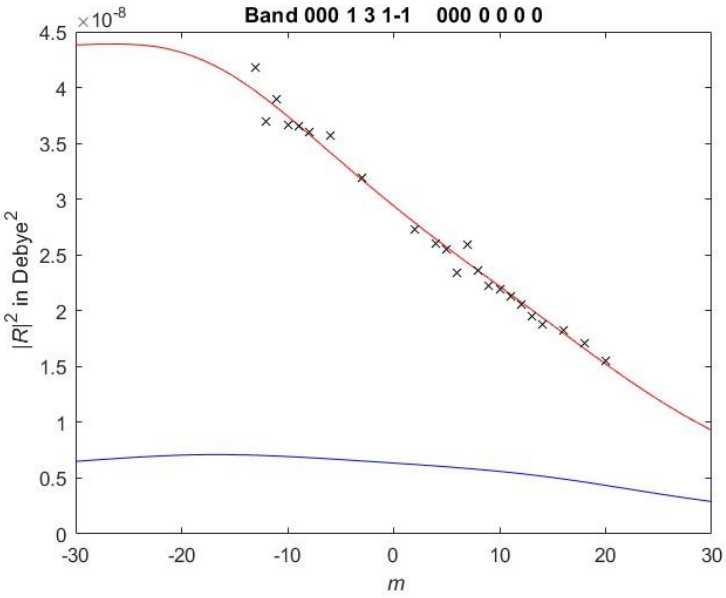

Fig.9. Vibration-rotation transition moments squared $|R|^2$ obtained for the $(\nu_4+3\nu_5)^0$ band. See Fig. 7 for legend.

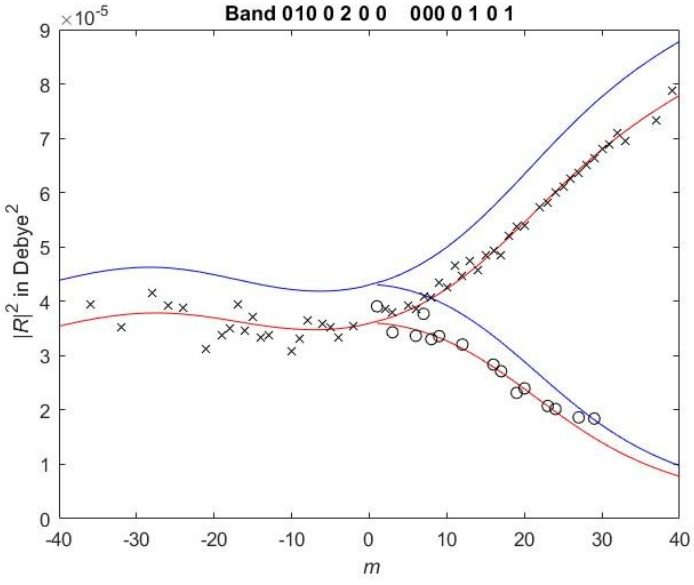

Fig.10. Vibration-rotation transition moments squared $|R|^2$ obtained for the $\nu_2+2\nu_5^0$ - ν_5^1 band. See Fig. 7 for legend.

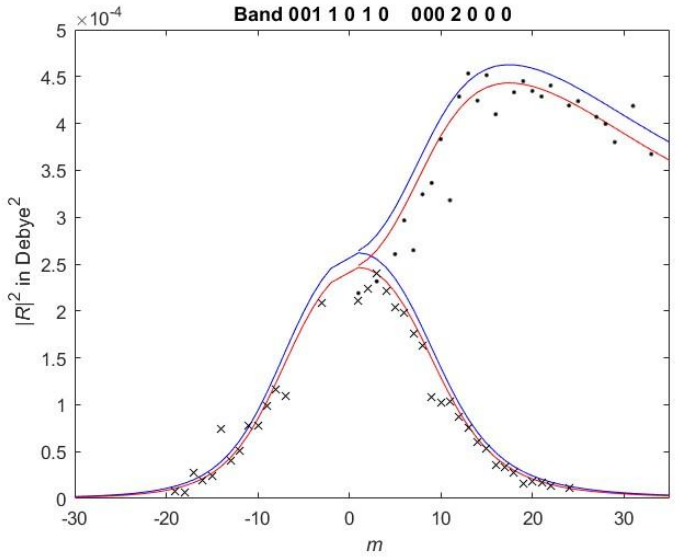

Fig.11. Vibration-rotation transition moments squared $|R|^2$ obtained for the $\nu_3+\nu_4^1$ - $2\nu_4^0$ band. See Fig. 7 for legend. Cross symbols for P_{ee} and R_{ee} sub-branches and dot symbols for Q_{fe} sub-branch have been used for measurements.

6. Generation of a line list for $^{12}C_2H_2$ in the $\Delta P = 4$ spectral region

A complete line list in the $\Delta P = 4$ spectral region has been generated for the 71 bands studied in this work, including the 5 strongest bands, already present in the 2020 edition of the HITRAN and GEISA databases, and the 14 bands previously studied in Ref. [1]. The line list covers the 2389-2890 cm^{-1} spectral range and contains 7515 transitions of $^{12}C_2H_2$ isotopologue.

One of the difficulties was to decide if extrapolations of measurements could be performed. As for line intensities, as explained in the previous Section, we are confident that the EDM model is able to accurately reproduce interpolated as well as extrapolated line intensities. However for line positions, the spectroscopic constants may lead to an inaccurate extrapolation as demonstrated in Figs. 2 and 3 (last two panels). Moreover, reproducing measurements at high J values using spectroscopic constants in the cases of perturbed bands is also not satisfactory (see Fig. 6 for example). In order to improve residuals between calculated and measured line positions for perturbed bands, we proposed in Section 4 to rescale the prediction of the EH model using polynomial expressions (see Section 4). Such empirical rescaling of the EH predictions may also lead to inaccurate extrapolations of the line positions (as with the spectroscopic constants). If the EH prediction is in good agreement with the measurement without rescaling, its extrapolated position values can be used with confidence. The situation has been evaluated individually for each band. Among the 71 bands presenting in our line list the positions have been generated by EH prediction only for 6 bands. For the other bands rescaled predictions or spectroscopic constants have been used to reproduce measurements with the best precision. The Table 4 summarizes the information on the contents of the recommended acetylene line list from this work. Interpolations were systematically performed. Concerning extrapolations, they have been performed only in a few cases where the upper level of the transition was measured through another sub-branch. For example, the calculation from the measurements in the P_{ee} sub-branch of the $\nu_3+2\nu_5^2$ - $(\nu_4+2\nu_5)^3$ band has been used to derive the line positions in the R_{ee} sub-branch for which no measurement is present. Extrapolations are indicated in the "sub-branch limits" column of the Table 4 by a "/" symbol. No extrapolation was done where the "/" symbol is absent. For example, for the Q_{ef} sub-branch of the $\nu_3+2\nu_5^2$ - $(\nu_4+2\nu_5)^1$I band (denoted 001 0 2 0 2_000 1 2-1 2) the measurements were obtained only up to $J = 6$ whereas the line positions were generated up to $J = 15$. In the column "Model" of Table 4, the model used for the line positions calculation is indicated by

"Pred" for prediction using EH model or by "Constants" for the use of spectroscopic constants from Table 1, or by "Pred_Cor" for corrected/rescaled EH model. The line intensities were calculated using EDM model with parameters from Table 3. Note that a line intensity cutoff equal to 10^{-28} cm/molecule has been applied in the present line list so that some interpolations to the lowest *J* values (with intensities lower than 10^{-28} cm/molecule) were ignored. In the last column of the Table are given uncertainties of calculations using HITRAN codes corresponding to absolute uncertainty ranges. Same codes are chosen for all transitions belonging to a band. From the comparisons between calculated and measured line positions, codes 2, 3 and 4 have been assigned to the line positions, corresponding to uncertainty ranges equal to 0.01− 0.1 cm^{-1}, 0.001− 0.01 cm^{-1} and 0.0001− 0.001 cm^{-1}, respectively. As for line intensities codes we decided to use RMS from Table 2: RMS values must be inside the uncertainty range defined by the code. For example, for the $(\nu_4+3\nu_5)^0$ band RMS value is equal to 3.11 % (see Table 2), and are between 2-5% (code 6 in HITRAN). Codes 5, 4 and 3 for intensities correspond to uncertainty ranges 5-10%, 10-20% and >20% respectively. For the bands included in HITRAN2020 (with a code 6 for intensities degraded to a code 5 for extrapolations), two sets of measurements are available. RMS values from Table 2 obtained for the observations of Ref. [2] are systematically smaller than those obtained for this work and could lead to uncertainties between 1 and 2% (code 7 in HITRAN) which will be an ultimate limit for accuracy due mainly to the knowledge of the concentration of $^{12}C_2H_2$ in the sample. We decided for these 5 bands to keep previously used code 6 (2-5%) that includes RMS values of both sets of measurements (Ref. [2] and this work).

For the broadening and shifting parameters polynomial expressions (functions of *J*) or default values (with associated uncertainty codes) described in the HITRAN 2008 edition [17] were used. The recommended line list (in HITRAN format) for the 71 bands of $^{12}C_2H_2$ studied in the present work is available as Supplementary Material II and is proposed to replace completely line list from databases in the $\Delta P = 4$ spectral region.

Table 4. The details of the line list construction in the ΔP=4 spectral region.

Band[a] Upper	Band[a] Lower	Sub-branch limits[b] P_{ee}	R_{ee}	Q_{ef}	P_{ff}	R_{ff}	Q_{fe}	Spectral range (in cm^{-1})	N^c	Model[d]	Uncertainty codes[e] Pos	Int
Bands present in HITRAN2020 and GEISA2020 databases												
000 3 1 1	-1 000 0 0 0 0	35	33	NA	NA	NA	--	2491-2654	69	Pred	4	6
001 0 0 0	0 000 1 0 1 0	41	39	39	NA	NA	NA	2568-2758	119	Pred_Cor	4	6
010 0 1 0	1 000 0 0 0 0	39	43	NA	NA	NA	43	2600-2793	125	Pred_Cor	4	6
010 1 1 1	-1 000 1 0 1 0	39	39	38	30	32	30	2585-2770	208	Pred_Cor(ee+ef)/Constants(ff+fe)	4	6
100 0 0 0	0 000 0 1 0 1	42	40	41	NA	NA	NA	2533-2729	123	Pred_Cor	4	6
Bands measured for the first time in the present work												
000 1 3 1	-1 000 0 0 0 0	21	19	NA	NA	NA	--	2710-2808	41	Pred_Cor	4	6
000 3 1 1	1 000 0 0 0 0	19	27	NA	NA	NA	--	2541-2654	47	Constants	4	5
000 4 1 1	-1 000 1 0 1 0	29	27	--	20	20	--	2500-2634	86	Constants	3	6
000 5 1 1	-1 000 2 0 0 0	23	17	NA	NA	NA	--	2540-2635	41	Pred_Cor	4	6
000 5 1 3	-1 000 2 0 2 0	23	21	4/20	24	24	5/20	2540-2635	124	Pred_Cor(ee)/Constants(ff+ef+fe)	3	6
001 0 1 0	1 000 1 1 1 1	25	28	31	29	29	32	2602-2742	168	Constants	4	6
001 0 1 0	1 000 1 1 1 -1	29	30	29	31	31	28	2599-2752	178	Pred_Cor	4	6
001 0 2 0	0 000 1 2 1 0	17	18	19	NA	NA	NA	2638-2726	54	Constants	3	5
001 0 2 0	0 000 1 2 -1 2	15	11	22	NA	NA	NA	2623-2688	48	Pred_Cor	4	5
001 0 2 0	2 000 1 2 1 0	--/11	11	20	--/14	14	13	2684-2722	77	Constants	3	6
001 0 2 0	2 000 1 2 1 2	11	--/11	16	14	--/14	15	2635-2697	69	Pred	3	5
001 0 2 0	2 000 1 2 -1 2	13	15	6/15	--/12	12	15	2638-2707	76	Pred	3	5
001 1 0 1	0 000 2 0 0 0	21	23	NA	NA	NA	33	2611-2716	77	Pred_Cor	4	6
001 1 0 1	0 000 2 0 2 0	35	35	36	34	34	23	2580-2747	191	Pred_Cor	4	6
001 1 1 1	1 000 2 1 0 1	20	20	13	23	23	14	2604-2715	107	Pred	3	6
001 1 1 1	1 000 2 1 2 1	12	16	25	19	15	24	2610-2697	96	Constants	3	6
001 1 1 1	-1 000 2 1 0 1	--	--	--	17	19	24	2617-2703	60	Pred_Cor	4	6
001 1 1 1	-1 000 2 1 2 -1	22	20	25	19	19	20	2616-2721	125	Constants	3	6
001 2 0 0	0 000 3 0 1 0	25	23	26	NA	NA	NA	2593-2710	74	Pred_Cor	3	6
001 2 0 2	0 000 3 0 1 0	15	17	16	10	14	29	2613-2691	95	Pred_Cor(ee+fe)/Constants(ff+ef)	3	5
001 2 0 2	0 000 3 0 3 0	29	27	26	24	26	19	2581-2715	136	Pred_Cor	3	6
010 0 2 0	0 000 0 1 0 1	36	38	33	NA	NA	NA	2601-2776	107	Pred_Cor	4	6
010 0 2 0	2 000 0 1 0 1	28	30	35	29	35	34	2626-2777	185	Pred_Cor(ee+ef)/Constants(ff+fe)	4	6
010 0 3 0	1 000 0 2 0 0	25	27	NA	NA	NA	23	2626-2750	75	Pred_Cor	4	6
010 0 3 0	1 000 0 2 0 2	19	21	20	24	26	27	2624-2745	131	Constants	3	6
010 0 3 0	3 000 0 2 0 2	19	25	28	20	24	27	2649-2757	131	Pred_Cor	4	6
010 1 1 1	1 000 1 0 1 0	19	23	38	28	34	31	2620-2762	167	Pred_Cor(ee+ef)/Constants(ff+fe)	4	6

010 1 2 1 0_000 1 1 1 1	22	20	27	25	21	28	2598-2710	137	Constants	3	5
010 1 2 1 0_000 1 1 1-1	22	--/22	33	33	31	20	2580-2734	161	Constants	3	6
010 1 2 1 2_000 1 1 1 1	16	22	27	15	23	26	2650-2743	117	Constants	4	6
010 1 2-1 2_000 1 1 1-1	16	18	27	27	29	20	2615-2749	137	Constants	4	6
010 2 1 0 1_000 2 0 0 0	19	21	NA	NA	NA	25	2630-2726	65	Pred_Cor	4	6
010 2 1 2 1_000 2 0 0 0	17	23	NA	NA	NA	31	2637-2733	64	Pred_Cor	4	6
010 2 1 2 1_000 2 0 2 0	--/15	15	22	10	14	8	2657-2719	72	Constants	4	6
010 2 1 2-1_000 2 0 0 0	19	23	NA	NA	NA	33	2601-2700	75	Pred_Cor	4	5
010 2 1 2-1_000 2 0 2 0	35	33	34	34	32	23	2565-2727	185	Pred_Cor(ee+fe)/Constants(ff+ef)	4	6
010 2 2 2 0_000 2 1 0 1	14	18	15	17	11	16	2609-2671	85	Constants	2	3
010 2 2 2-2_000 2 1 0 1	10	10	19	17	17	24	2599-2682	97	Pred_Cor(ff)+Pred(ee+fe+ef)	2	3
010 3 1 1-1_000 3 0 1 0	23	23	28	--	--	--	2580-2691	74	Pred_Cor	3	6
010 3 1 3-1_000 3 0 1 0	13	19	9	10	14	27	2600-2676	86	Pred_Cor(fe)/Constants(ee+ff+ef)	3	3
010 3 1 3-1_000 3 0 3 0	22	25	22	26	20	15	2571-2692	118	Pred_Cor	3	6
100 0 1 0 1_000 2 0 2 0	15	11	20	18	10	15	2818-2890	83	Constants	3	5
100 0 2 0 0_000 0 3 0 1	26	22	21	NA	NA	NA	2566-2683	69	Pred_Cor	4	6
100 0 2 0 2_000 0 3 0 1	14	14	23	19	13	18	2590-2675	95	Pred	3	3
100 0 2 0 2_000 0 3 0 3	22	18	23	21	19	26	2566-2666	117	Pred_Cor	4	5
100 1 1 1 1_000 1 2 1 0	15	13	24	18	20	17	2592-2680	101	Pred	3	5
100 1 1 1-1_000 1 2-1 2	--	--	--	26	22	25	2557-2674	73	Pred_Cor	4	5
100 2 0 0 0_000 2 1 0 1	22	18	27	NA	NA	NA	2551-2650	67	Pred_Cor	3	5
100 2 0 0 0_000 2 1 2-1	26	26	15	NA	NA	NA	2562-2687	67	Pred_Cor	3	5
100 2 0 2 0_000 2 1 0 1	14	16	--	--	--	22	2576-2650	49	Constants	2	3
100 2 0 2 0_000 2 1 2 1	24	17	27	21	21	22	2549-2657	120	Pred_Cor(ee+Qef)/Constants(ff+Qfe)	4	5
100 2 0 2 0_000 2 1 2-1	6	8	23	23	23	22	2570-2681	99	Pred_Cor(ee+Qef)/Constants(ff+Qfe)	3	6

Bands previously measured in Ref. [1]

000 3 1 3-1_000 0 0 0 0	37	33	NA	NA	NA	NA	2469-2637	68	Pred_Cor	4	6
000 3 2 3 0_000 0 1 0 1	24	23	--	27	29	--	2488-2622	95	Constants	3	6
000 3 2 3-2_000 0 1 0 1	32	27	3	27	21	6	2458-2599	114	Constants	3	6
000 3 2-1 2_000 0 1 0 1	30	26	7	27	23	6	2490-2624	117	Pred_Cor	3	6
000 4 1 2-1_000 1 0 1 0	31	29	11	32	32	13	2507-2659	146	Pred_Cor	4	6
000 4 2 2-2_000 1 1 1-1	20	19	--	17	15	--	2511-2607	73	Pred_Cor	4(ee)/2(ff)	6
010 2 0 0 0_000 0 1 0 1	22	20	29	NA	NA	NA	2399-2501	71	Pred_Cor	4	5
010 2 0 2 0_000 0 1 0 1	24	30	33	15	21	22	2389-2515	138	Pred_Cor(ee+ef)/Constants(ff+fe)	3	6
100 0 1 0 1_000 0 2 0 0	32	33	NA	NA	NA	31	2557-2711	96	Pred_Cor	4	6
100 0 1 0 1_000 0 2 0 2	31	28	34	34	32	35	2545-2704	188	Constants	3	6
100 1 0 1 0_000 1 1 1 1	32	29	33	33	33	36	2538-2696	190	Pred_Cor(ee+fe)/Constants(ff+ef)	3	6
100 1 0 1 0_000 1 1 1-1	34	34	33	31	29	32	2549-2711	193	Pred_Cor(ee+fe)/Constants(ff+ef)	3	6
100 1 1 1 1_000 1 2 1 2	23	21	26	22	22	25	2555-2663	127	Pred_Cor(ef+fe)/Constants(ff+ee)	3	6
100 1 1 1-1_000 1 2 1 0	25	25	26	--	--	--	2564-2684	76	Pred_Cor	4	6

[a] Normal mode labeling of the vibrational states: $V_1V_2V_3V_4V_5\ \ell_4\ \ell_5$

[b] The numbers correspond to maximum J_{low} values measured for each sub-branch. Notation "NA" refers to non existing sub-branch, whereas the notation "--" corresponds to the cases where no observation is performed for the sub-branch. Extrapolations are indicated by a "/" symbol followed by the maximum extrapolated *J* values.

[c] *N* is the number of transitions generated for each band in the recommended line list.
[d] The model used to generate line positions in the present line list: “Pred” states for prediction using EH model, “Constants” for the use of spectroscopic constants from Table 1, and “Pred_Cor” for corrected/rescaled EH model.
[e] The uncertainty codes according to HITRAN uncertainty ranges

In order to check the quality of the present line list, a synthetic spectrum has been calculated under experimental conditions corresponding to the largest optical absorption path (1057.95 m). An extract of the comparison between experimental and synthetic spectrum is presented in Fig. 12. As one can see the most of the observed transitions are well reproduced by the present line list except for transitions belonging to $^{12}C^{13}H_2$ and $^{12}C_2HD$ isotopologues not studied in the present work. The line positions of these isotopologues reported in Ref. [18] and [19], respectively, were used in the present work for assignments.

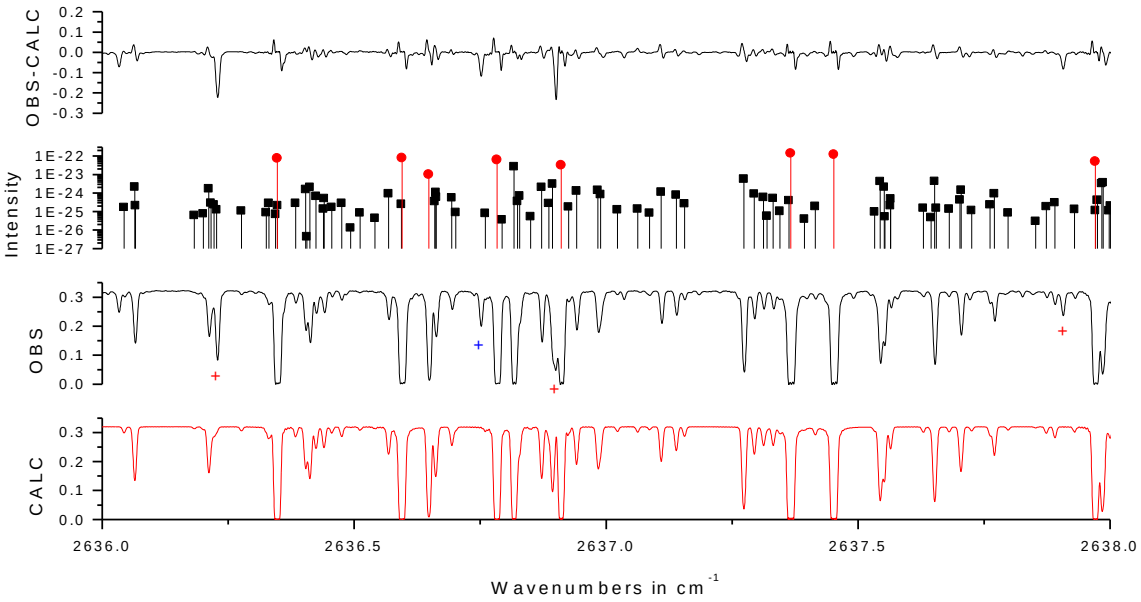

Fig.12. Comparison between synthetic (CALC) and observed (OBS) spectra in the 2636-2638 cm^{-1} spectral domain. The OBS-CALC residuals are given on the first panel. On the second panel the recommended line list is plotted as a stick plot in a log scale for intensities (in cm/molecule), the transitions included in the 2020 edition of the HITRAN and GEISA databases are shown in red. The two latest panels represent the experimental spectrum (OBS) recorded with absorption path equal to 1057.95 m and corresponding synthetic (CALC) spectrum. In the third panel transitions belonging to the $^{12}C^{13}H_2$ and $^{12}C_2HD$ isotopologues are indicated by red and blue crosses respectively.

6. Conclusion

The present work is finalizing our study on $^{12}C_2H_2$ transitions in the $\Delta P = 4$ spectral region using Fourier transform spectra with long absorption path. Those spectra allowed to identify and analyze 71 bands including the 5 bands given in the 2020 edition of the HITRAN and GEISA databases. The line positions were modeled using either set of spectroscopic constants or global effective Hamiltonian model (most of the time rescaled). The intensity calculations with the effective dipole moment operator demonstrated the good agreement with the observation. Using these calculations a recommended line list, including some interpolations and extrapolations, has been generated and is proposed for updating the whole $\Delta P = 4$ spectral region in the HITRAN and GEISA spectroscopic databases.

A forthcoming study, the third and the last of the series, will aim to complete the present work by investigating observed bands of $^{12}C^{13}CH_2$ and $^{12}C_2HD$ isotopologues.

Acknowledgements

This work is supported by CNRS (France) in the framework of the Collaborative Project SAMIA (Spectroscopie d'Absorption des Molécules d'Intérêt Atmosphérique). The researchers from V.E. Zuev Institute of Atmospheric Optics of Siberian Branch of the Russian Academy of Sciences are grateful for financial support by the Ministry of Science and Higher Education of the Russian Federation. The experimental part of the work was carried out using the equipment of the Center for Collective Use "Atmosphere" with partial financial support from the Ministry of Education and Science of Russia (Agreement No. 075–15–2021–661).

References

[1] Jacquemart, Lyulin OM, Solodov AM, Petrova TM, Solodov AA, Perevalov VI. New acetylene line list near 3.8-μm - Part I. JQSRT 2023;295:108413.

[2] Jacquemart D, Lacome N, Mandin JY, Dana V, Lyulin OM, Perevalov VI. Multispectrum fitting of line parameters for $^{12}C_2H_2$ in the 3.8-μm spectral region. JQSRT 2007;103:478-95.

[3] Lyulin OM, Perevalov VI, Mandin JY, Dana V, Gueye F, Thomas X, et al. Line intensities of acetylene: measurements in the 2.5-μm spectral region and global modelling in the ΔP=4 and 6 series. JQSRT 2007;103:496-523.

[4] Lyulin OM, Perevalov VI. ASD-1000: high-resolution, high-temperature acetylene spectroscopic databank. JQSRT 2017;201:94-103.

[5] Lyulin OM, Perevalov VI. Global modelling of vibration-rotation spectra of acetylene molecule. JQSRT 2016;177:59-74.

[6] Lyulin OM. Determination of Spectral Line Parameters from Several Absorption Spectra with the MultiSpectrum Fitting Computer Code. Atmospheric and Oceanic Optics 2015 ;28:487–95.

[7] Gordon IE, Rothman LS, Hargreaves RJ, Hashemi R, Karlovets EV et al. The HITRAN2020 molecular spectroscopic database. JQSRT 2022;277:107949.

[8] Guelachvili G. Distorsions in Fourier Spectra and diagnosis. In: Vanasse GA, editor. Spectrometric techniques, Vol. II. New York: Academic Press; 1981. p. 1–62.

[9] Gamache RR, Roller C, Lopes E, Gordon IE, Rothman LS, et al. Total internal partition sums for 166 isotopologues of 51 molecules important in planetary atmospheres: Application to HITRAN 2016 and beyond. JQSRT 2017;203:70-97.

[10] Delahaye T, Armante R, Scott NA, Jacquinet-Husson N, Chédin A et al. The 2020 edition of the GEISA spectroscopic database. J Mol Spectrosc 2021;380:111510.

[11] Jacquemart D, Lyulin OM, Perevalov VI. Recommended acetylene line list in the 20 − 240 cm^{-1} and 400 − 630 cm^{-1}: New measurements and global modeling. JQSRT 2017;203:440-53.

[12] Lyulin OM, Mondelain D, Béguier S, Kassi S, Vander Auwera J, Campargue A. High sensitivity absorption spectroscopy of acetylene by CRDS between 5851 and 6341 cm^{-1}. MolPhys2014;112:2433–44.

[13] Lyulin OM, Vasilchenko S, Mondelain D, Kassi S, Campargue A. The acetylene spectrum in the 1.45 μm window (6627-7065 cm^{-1}). JQSRT 2020;253:107057.

[14] Gomez L, Jacquemart D, Lacome N, Mandin JY. New line intensity measurements for $^{12}C_2H_2$ around 7.7 μm and HITRAN format line list for applications. JQSRT 2010;111:2256-64.

[15] Pliva J. Molecular constants for the bending modes of acetylene $^{12}C_2H_2$. J Mol Spectrosc 1972;44:165-82.

[16] Perevalov VI, Lyulin OM, Teffo J.-L. Global treatment of line intensities of vibrational-rotational transitions of the acetylene molecule. Approach and design formulas. Atmos. Oceanic Opt. 2001;14,730-9.

[17] Jacquemart D, Mandin JY, Dana V, Claveau C, Vander Auwera J, Herman M, Rothman LS, Régalia-Jarlot L, Barbe A. The IR acetylene spectrum in HITRAN: update and new results. JQSRT 2003;82:363-82.

[18] Di Lonardo G, Baldan A, Bramati G, Fusina L. The Infrared Spectrum of $^{12}C^{13}CH_2$: The Bending States up to $\nu_4+\nu_5 = 4$. J Mol Spectrosc 2002;213:57-63.

[19] Fusina L, Tamassia F, Di Lonardo G. The infrared spectrum of $^{12}C_2HD$: the stretching–bending combination bands in the 1800–4700 cm^{-1} region. Molelcuar Physics 2005;103:2613-20.